



저작자표시-비영리-변경금지 2.0 대한민국

이용자는 아래의 조건을 따르는 경우에 한하여 자유롭게

- 이 저작물을 복제, 배포, 전송, 전시, 공연 및 방송할 수 있습니다.

다음과 같은 조건을 따라야 합니다:



저작자표시. 귀하는 원저작자를 표시하여야 합니다.



비영리. 귀하는 이 저작물을 영리 목적으로 이용할 수 없습니다.



변경금지. 귀하는 이 저작물을 개작, 변형 또는 가공할 수 없습니다.

- 귀하는, 이 저작물의 재이용이나 배포의 경우, 이 저작물에 적용된 이용허락조건을 명확하게 나타내어야 합니다.
- 저작권자로부터 별도의 허가를 받으면 이러한 조건들은 적용되지 않습니다.

저작권법에 따른 이용자의 권리는 위의 내용에 의하여 영향을 받지 않습니다.

이것은 [이용허락규약\(Legal Code\)](#)을 이해하기 쉽게 요약한 것입니다.

[Disclaimer](#)

Ph. D. Dissertation

**Synthesis of $\text{YVO}_4\text{:Eu}^{3+}$ phosphors and the
effect of nano-sized SiO_2 on the optical
properties**

Advisor

Shinhoo Kang

By

Seyed Mahdi Rafiaei

Submitted in fulfilment of the requirements for the degree
of

Doctor of Philosophy

Department of Materials Science and Engineering

Graduate School

Seoul National University

2017

Synthesis of $\text{YVO}_4:\text{Eu}^{3+}$ phosphors and the effect of nano-sized SiO_2 on the optical properties

지도교수 강 신 후

이 논문을 공학박사학위논문으로 제출함

2017년 8월


서울대학교 대학원


재료공학부


Seyed Mahdi Rafiaei

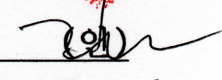
Seyed Mahdi Rafiaei의 박사학위논문을 인준함

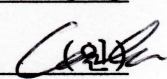
2017년 8월

위원장 홍 성 현 

부위원장 남 기 태 

위 원 강 신 후 

위 원 김 용 선 

위 원 이 관 형 

This dissertation is dedicated to my wife.

Abstract

In this work, bulk sized $\text{YVO}_4:\text{Eu}^{3+}$ phosphor was synthesized via simple solid state method in air atmosphere at 1100 °C, which has a variety of applications in the fields of lighting and solar cells. All these applications are possible due to the proper designation of particle size, morphology and defects control of surface through the experimental parameters. Referring to the literatures, synthesis of the $\text{YVO}_4:\text{Eu}^{3+}$ phosphors in the air atmosphere, results in the formation of many defects and then the optical properties are suppressed. For improvement of luminescence properties, the surface of $\text{YVO}_4:\text{Eu}^{3+}$ phosphor was coated by a thin layer of SiO_2 through sol-gel (with a source of TEOS) and then obtained morphology and photoluminescence properties were investigated in details. It was found that silica coating yields an increase in luminescence intensity of the $\text{YVO}_4:\text{Eu}^{3+}$ phosphors due to the reduction of reflection of excitation light and the maximum amounts of emission intensity was obtained with 1 wt% silica coating when the thickness of silica on the surface is in the range of 20-50 nm. Another effective mechanism for luminescence improvement is the decrease of surface defects by coating the surface of phosphor. The ESR analyses approved that with coating of a layer of silica on the surface of $\text{YVO}_4:\text{Eu}^{3+}$ phosphor, the amounts of oxygen vacancy defects reduced remarkably. Furthermore, the coating of $\text{YVO}_4:\text{Eu}^{3+}$ phosphors by silica enhanced the chemical and thermal stability too. Also, in another procedure and to study the effect of SiO_2 core on

YVO₄:Eu³⁺ phosphors, the YVO₄:Eu³⁺@SiO₂ phosphors were synthesized through sol-gel process too. It was found that after 5 times coating of YVO₄:Eu³⁺ on SiO₂ core, the emission intensity is significantly comparable to that of pure YVO₄:Eu³⁺ phosphors. In addition, although the coating of YVO₄:Eu³⁺@SiO₂ phosphors with silica resulted in decrease of luminescence properties but the thermal quenching and chemical stability were enhanced.

Key words: Luminescence, Silica, solid state, sol-gel, excitation and emission.

Contents

Abstract	i
Contents	iii
List of Figures	vii
List of Tables	xi
List of Appendixes	xi
I. Introduction.....	1
1.1. Phosphors at a glance.....	1
1.1.1. Synthesis of phosphors.....	2
1.2. YVO ₄ phosphors.....	3
II. Synthesis of Bulk YVO₄: Eu³⁺ Phosphor Materials.....	6
2.1. Introduction.....	6
2.2. Experimental.....	7
2.2.1. Preparation.....	7
2.2.2. Characterization.....	7

2.3. Results and discussion	8
2.3.1. XRD, SEM, HRTEM Studies.....	8
2.3.2. PL Analysis.....	10
2.3.2.1. Un-doped YVO ₄ phosphor.....	10
2.3.2.2. YVO ₄ : Eu ³⁺ phosphor.....	12
2.3.3. Raman Analysis.....	18
2.4. Summary and Conclusion	20
 III. Coating of YVO₄: Eu³⁺ phosphors with silica.....	21
 3.1. Introduction.....	21
3.2. Experimental.....	26
3.2.1. Preparation.....	26
3.2.1.1. YVO ₄ : Eu ³⁺ Phosphors Synthesis.....	26
3.2.1.2. Coating of YVO ₄ : Eu ³⁺ phosphors with silica.....	26
3.2.2. Characterization.....	28
3.3. Results and discussion.....	28
3.3.1. XRD Analysis	28
3.3.2. FESEM Observations.....	30
3.3.3. TEM Observations	35
3.3.4. XPS Analysis.....	38
3.3.5. FT- IR Analysis	43

3.3.6. PL Analysis.....	45
3.3.6.1. Reflection.....	47
3.3.6.2. Quantum Yield.....	50
3.3.7. Chemical Stability.....	52
3.3.7.1. Water Degradation.....	52
3.3.7.2. Acid Degradation.....	56
3.3.8. Thermal quenching.....	59
3.3.9. ESR Analysis.....	64
3.4. Summary and conclusion.....	66
 IV. Core shell $\text{YVO}_4:\text{Eu}^{3+}@\text{SiO}_2$ phosphors.....	67
 4.1 Introduction.....	67
4.2. Experimental.....	69
4.2.1. Synthesis of silica cores.....	69
4.2.2. Synthesis of $\text{SiO}_2@ \text{Y}_{0.96}\text{Eu}_{0.04}\text{VO}_4$ core-shell phosphors.....	69
4.3. Results and discussion.....	72
4.3.1. XRD Analysis.....	72
4.3.2. FESEM Observations	74

4.3.3. HRTEM Observations	76
4.3.4. FT- IR Analysis	78
4.3.5. PL Analysis	80
4.3.6. SiO ₂ coated YVO ₄ :Eu ³⁺ @SiO ₂ phosphors.....	84
4.3.6.1. XRD Analysis.....	85
4.3.6.2. FESEM Observation.....	86
4.3.6.3. HRTEM Observation.....	87
4.3.6.4. PL Analysis	89
4.3.6.5. Chemical Stability.....	90
4.3.6.6. Thermal quenching.....	92
4.4. Summary and conclusion.....	95
V. Overall Conclusion.....	96
Appendix.....	98
References	99
Acknowledgement	110

List of Figures

Chapter I:

Fig. 1.1. Schematic drawing of the Coordination of Yttrium and Vanadium with Oxygen atoms.

Chapter II:

Fig.2.1. (a) XRD spectra, (b) HRTEM, (c) SEM and (d) EDS spectra of YVO_4 : Eu^{3+} phosphor synthesized via solid state at 1100 °C.

Fig.2.2. Photoluminescence excitation and emission spectra of combustion synthesized YVO_4 host at room temperature.

Fig.2.3. Photoluminescence (a) excitation and (b) emission of YVO_4 : Eu^{3+} phosphors synthesized via solid state at 1100 °C.

Fig. 2.4. Energy level diagram of Eu^{3+} ions.

Fig.2.5. Schematic drawing of water molecules on the surface of YVO_4 nanocrystals.

Fig.2.6. Raman spectra of the YVO_4 : Eu^{3+} nano-phosphor after calcination at 600 °C and 1000 °C.

Chapter III:

Fig.3.1. Non uniform coating of SiO_2 on the surface of (a), (b), (c) Y_2O_3 : Eu^{3+} and (d) CeO_2 particles.

Fig.3.2. XRD spectra of sol gel synthesized YVO_4 : Eu^{3+} phosphors with different concentrations of SiO_2 .

Fig.3.3. FESEM images of $\text{YVO}_4\text{:Eu}^{3+}$ phosphors with (a) 0 wt% SiO_2 , (b) 0.5 wt% SiO_2 , (c) 1 wt% SiO_2 and (d) 2 wt% SiO_2 .

Fig. 3.4 FESEM images of silica coating particles on the surface $\text{YVO}_4\text{:Eu}^{3+}$ phosphors (in the sample coated with 1 wt% SiO_2).

Fig. 3.5 FESEM images of non uniform dispersion of SiO_2 particles in the $\text{YVO}_4\text{:Eu}^{3+}$ phosphors coated with 4wt% SiO_2 .

Fig.3.6. TEM images of $\text{YVO}_4\text{:Eu}^{3+}$ phosphors coated with a layer of SiO_2 (1wt% SiO_2).

Fig.3.7. TEM images of non-uniform silica coating on the surface of $\text{YVO}_4\text{:Eu}^{3+}$ phosphors.

Fig.3.8 XPS spectra of $\text{YVO}_4\text{:Eu}^{3+}$ / 1 wt% SiO_2 phosphors.

Fig.3.9 Silicon peaks in the XPS spectra of $\text{YVO}_4\text{:Eu}^{3+}$ / 1 wt% SiO_2 phosphors.

Fig.3.10. Yttrium peaks in the XPS spectra of $\text{YVO}_4\text{:Eu}^{3+}$ / 1 wt% SiO_2 phosphors.

Fig.3.11. Vanadium and oxygen peaks of $\text{YVO}_4\text{:Eu}^{3+}$ / 1 wt% SiO_2 phosphors.

Fig.3.12. FT-IR spectra of $\text{YVO}_4\text{:Eu}^{3+}$ phosphors with 1 wt% SiO_2 after calcinations at $T=400\text{ }^\circ\text{C}$, $T=900\text{ }^\circ\text{C}$ for 3h.

Fig.3.13 FT-IR spectra of $\text{YVO}_4\text{:Eu}^{3+}$ phosphors with 1 wt% SiO_2 after calcinations at $T=400\text{ }^\circ\text{C}$, $T=900\text{ }^\circ\text{C}$ for 3h.

Fig.3.14. Photoluminescence excitation of $\text{YVO}_4\text{:Eu}^{3+}$ phosphor.

Fig.3.15. Photoluminescence emission spectra $\text{YVO}_4\text{:Eu}$ phosphors with different concentrations of SiO_2 .

Fig.3.16. Strong reflection of bared $\text{YVO}_4:\text{Eu}^{3+}$ phosphors under excitation.

Fig.3.17. Weak reflection of bared $\text{YVO}_4:\text{Eu}^{3+}$ phosphors under excitation.

Fig.3.18. Photoluminescence excitation spectra of $\text{YVO}_4:\text{Eu}^{3+}$ phosphors (a) with 1 wt% SiO_2 , (b) without SiO_2 and (c) the combination of parts (a) and (b) after different time of immersion in water.

Fig.3.19. FESEM images of $\text{YVO}_4:\text{Eu}$ phosphors with (a), (b) 0 wt% SiO_2 , (c), (d) 2 wt% SiO_2 after immersing in acid for 20 min.

Fig.3.20. The schematic of charge transfer between ground and excited states.

Fig.3.21 Temperature dependent Photoluminescence emission spectra of $\text{YVO}_4:\text{Eu}^{3+}$ phosphors (a) without 1 wt% SiO_2 , (b) with SiO_2 and (c) the combination of parts (a) and (b).

Fig.3.22 ESR spectra of $\text{YVO}_4:\text{Eu}^{3+}$ phosphors in the cases of bare and coated with 1 wt% SiO_2 .

Chapter IV:

Fig.4.1. Schematic view of core-shell procedure for $\text{SiO}_2@\text{Y}_{0.96}\text{Eu}_{0.04}\text{VO}_4$ phosphors.

Fig4.2. XRD spectra of (a) SiO_2 core and (b) Core shell $\text{YVO}_4:\text{Eu}^{3+}@\text{SiO}_2$ phosphors.

Fig4.2. XRD spectra of (a) SiO_2 core and (b) Core shell $\text{YVO}_4:\text{Eu}^{3+}@\text{SiO}_2$ phosphors.

Fig.4.4 HRTEM images of (a) SiO_2 core, (b) Core shell $\text{YVO}_4:\text{Eu}^{3+}@\text{SiO}_2$ phosphors, (c) interface of core/shell and (d) SAED of $\text{YVO}_4:\text{Eu}^{3+}@\text{SiO}_2$ phosphors.

Fig.4.5 FT-IR spectra of SiO_2 core, Core shell $\text{YVO}_4:\text{Eu}^{3+}@\text{SiO}_2$ phosphors and pure $\text{YVO}_4:\text{Eu}^{3+}$ phosphors.

Fig.4.6 PL (a) excitation and (b) emission spectra of Core shell $\text{YVO}_4:\text{Eu}^{3+}@\text{SiO}_2$ phosphors after 2 times of coating.

Fig.4.7. The photoluminescence emission intensity of $\text{YVO}_4:\text{Eu}^{3+}@\text{SiO}_2$ phosphors as a function of the number of coatings (N).

Fig. 4.8 XRD spectra of $\text{SiO}_2@Y_{0.96}\text{Eu}_{0.04}\text{VO}_4$ with different amounts of silica coating: (a) 0 wt%, (b) 1 wt% and (c) 2 wt%.

Fig. 4.9 FESEM images of $\text{SiO}_2@Y_{0.96}\text{Eu}_{0.04}\text{VO}_4$ coated with 1 wt% silica at different magnifications.

Fig. 4.10 HRTEM images of $\text{SiO}_2@Y_{0.96}\text{Eu}_{0.04}\text{VO}_4$ coated with 1 wt% silica at different magnifications.

Fig. 4.11 Photoluminescence emission properties of SiO_2 coated $\text{YVO}_4:\text{Eu}^{3+}@\text{SiO}_2$ phosphors with different amounts of silica.

Fig. 4.12 Temperature dependent Photoluminescence emission spectra of $\text{YVO}_4:\text{Eu}^{3+}$ phosphors (a) without 1 wt% SiO_2 , (b) with SiO_2 and (c) the combination of parts (a) and (b).

List of Tables

Chapter I:

Table 1.1 Physical properties of YVO_4

Chapter II:

Table 2.2 Number of emission bands for the Eu^{3+} ion.

Chapter III:

Table 3.1 Electronegativity of elements.

Table 3.2 The quantum efficiencies for bare and coated $\text{YVO}_4:4\%\text{Eu}^{3+}$.

Table 3.3 the amounts of elements (ppm) of bare and coated $\text{YVO}_4:4\%\text{Eu}^{3+}$ phosphors in the acid mixture solution.

List of Appendixes

Table 1 Physical properties of SiO_2 (appendix)

I. Introduction

1.1. Phosphors at a glance

A phosphor compound mostly is a substance material with the phenomenon of luminescence. This includes both phosphorescent materials, which show a slow decay in brightness (> 1 ms) and fluorescent materials, where the emission decay takes place over tens of nanoseconds. Phosphors are usually made from a suitable host material with an added activator. The host materials have a wide variety but they can typically be oxides, nitrides and oxynitrides, sulfides, selenides, halides or silicates of zinc, cadmium, manganese, aluminium, silicon, or various rare earth metals [1]. Phosphor materials may be used in a variety of applications ranging from the fluorescent lamp to the luminescence immunoassay. These materials essentially convert one type of energy into visible radiation and hence, phosphor materials are called optical transducer. They are generally crystalline in nature. There has been an increasing interest in rare-earth phosphors since 1980 as evidenced from the published international technical reports and reviews [2-8]. Phosphors activated by rare earth ions exhibit some peculiarities. In the energy level diagram of the rare-earth, luminescence processes often correspond to electronic transitions within the incompletely filled 4f shell, which is extensively shielded from host lattice. Consequently, these phosphors have narrow band spectra which are to a great

extent independent of the nature of the host lattice. Because of the low interaction with the crystal field, luminescence quantum yield of phosphors activated with rare earths is often high compared to other phosphors. Quenching occurs only at higher temperatures or higher activator concentrations [9]. There are a variety of methods for synthesis of phosphors but proper optimization of the growth process allows avoiding the annealing [10]. Always it is tried to change the composition of phosphors to eliminate some toxic elements, such as beryllium, cadmium, or thallium, formerly used [11].

1.1.1. Synthesis of Phosphors

There are a wide variety of synthesizing methods to produce phosphor materials. It is well known that synthesis method affects the microstructure and optical properties. Since in this work, solid state and sol-gel methods were employed to produce phosphor materials, these two methods are explained in details.

Solid State Synthesis: The solid state synthesis method is a very common method since it is not complicated and sensitive to the procedure steps. Mostly, oxide powders are mixed well and undergo high temperatures for enough time. Although this method has some advantages including simplicity but it has some drawbacks too. Firstly, the obtained average size of particles is relatively large and it is usually larger than 5 μm [12]. Secondly, it is usually time consuming and costly since the solid precursor should be heated at high temperature for several hours.

Sol-Gel Synthesis: The synthesis process involves conversion of monomers into a colloidal solution (sol) that acts as the precursor for an integrated network (or gel) of either discrete particles or network polymers. Typical precursors are metal alkoxides. The obtained particle size is very different depending on the procedure parameters.

1.2. YVO₄ Phosphors

Yttrium orthovanadate belongs to the group of oxide compounds crystallizing in the ZrSiO₄ zircon structure with tetragonal space group I 41/amds (D_{4h}^{19}), space group No. 141 with the atomic positions that are seen in Table 1.1. A unit cell of Yttrium orthovanadate contains four YVO₄ with a total of 24 atoms and the trivalent rare-earth ion is coordinated eightfold with oxygen and has the point group symmetry D_{2d} . It is arranged at the center of a tetrahedron formed by four oxygen atoms. This tetrahedron is shorter along the c axis than the corresponding dimensions perpendicular to the c axis and thus irregular, causing the reduction to D_{2d} symmetry. In other words, the V⁵⁺ ions are tetrahedrally coordinated by oxygen. The space between the isolated VO₄ tetrahedral units is occupied by Y³⁺ ions. As it is shown in Fig. 1.1, the Y ion is eight-fold coordinated by oxygen atoms, forming dodecahedral cages. In the doped YVO₄, the trivalent rare-earth activator ions substitute for Y. It's ideal for optical polarizing components such

as fibre optical isolators, beam displacers and circulators. YVO_4 is one of the most effective and advanced materials the production of diode pumped lasers. Also, the literatures show that Eu^{3+} doped YVO_4 has been a very promising and attractive red phosphor in the fields of lighting.

Table 1.1 Physical properties of YVO_4

Chemical Name	Yttrium Vanadate
Structural Formula	YVO_4
Crystal Structure	Tetragonal
Lattice Parameters	$a = b = 7.12 \text{ \AA}$, $c = 6.29 \text{ \AA}$
Lattice Angles	$\alpha = \beta = \gamma = 90^\circ$
Density	4.22 g/cm^3
Thermal Conductivity	C: 5.23 W/m/k ; $^{\wedge}\text{C}$ axis = 5.10 W/m/k
Y atom Positions	$X=0, Y=0, Z=0$
V atom Positions	$X=0, Y=0, Z=0.5$
O atom Positions	$X=0, Y=0.19, Z=0.35$

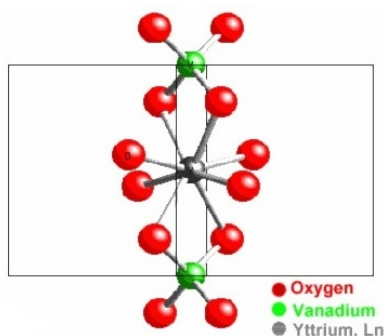


Fig. 1.1 Schematic drawing of the Coordination of Yttrium and Vanadium with Oxygen atoms.

Yttrium orthovanadate (YVO_4) has been extensively used as an excellent polarizer and laser host material whereas Eu^{3+} doped YVO_4 has been used as a red phosphor in color television and cathode ray tubes (CRTs) based on its high brightness and luminescence efficiency [13]. Even though at low temperatures, un-doped Yttrium orthovanadate shows excitation and emission bands centered at 330 and 420 nm, respectively, which are because of the $^1\text{A}_1 \rightarrow ^1\text{T}_1$ and $^3\text{T}_1 \rightarrow ^1\text{A}_1$ transitions of the vanadate group [14]. Un-doped YVO_4 is also used to make efficient high-power polarizing prisms similar to Glan–Taylor prisms. As mentioned elsewhere, it was already shown that YVO_4 material can be used as an effective host lattice for many of rare earth elements such as Eu, Sm, Dy and Er [15].

II. Synthesis of Bulk YVO₄: Eu³⁺ Phosphor Materials

2.1. Introduction

As it was explained in details, YVO₄ is a very well known and common host lattice for phosphors and specially the rare earth doped phosphors. A broad band in the range of 250–350 nm has been reported in the photoluminescence excitation (PLE) spectrum and this specification has attracted many researchers to study about YVO₄ materials. In this investigation, Eu³⁺ element was selected because of its interesting properties and applications in the field of lighting and solar cells. Since the ionic radius of Eu³⁺ ($r=0.095$ nm) is close to that of Y³⁺ ($r=0.089$ nm), it can be expected that this element will be more possibly substituted for the Y³⁺ sites without any inversion symmetry. This lack of inversion symmetry is the advantageous for the luminescence performance of trivalent rare earth ions, increasing the radiative rate constant, thus resulting in higher quantum yields [16]. On the other side, surface defect is one of the main problems that suppress the luminescence properties. Recently, Liusai and his colleagues reported that through post calcinations under air atmosphere, many oxygen vacancy defects have been formed on the surface of YVO₄ phosphors [17]. They employed electro paramagnetic resonance (EPR) analysis to prove the formation of V⁴⁺ ions instead of V⁵⁺ on the surface that is a strong evidence for the formation of oxygen vacancies. In this part, YVO₄: Eu³⁺ phosphor synthesized via a conventional solid state method.

2.2. Experimental

2.2.1. Preparation

To synthesize $\text{YVO}_4:\text{Eu}^{3+}$ phosphor, analytical grades of yttrium oxide (Y_2O_3), vanadium oxide (V_2O_5), europium oxide (Eu_2O_3) were purchased from Aldrich Company. In a typical procedure, 1 g of yttrium oxide, 0.84 g of vanadium oxide and 0.065 g of europium oxide were mixed and ground by pestle at least for 30 min in a mortar. The obtained powder mixture was synthesized at 1100 °C for 2h in an electrical tube furnace. After calcinations, the mixture was ground again sufficiently.

2.2.2. Characterization

For the study of the microstructure and photoluminescence characteristics of $\text{YVO}_4:\text{Eu}^{3+}$ phosphors, SEM and FESEM microscopes, XRD, FTIR, XPS and PL machines were employed.

2.3. Results and discussion

2.3.1. XRD, SEM, HRTEM Studies

Fig. 2.1 shows the XRD spectra, HRTEM, SEM and EDS spectra of $\text{YVO}_4:\text{Eu}^{3+}$ phosphor synthesized via solid state at 1100 °C.

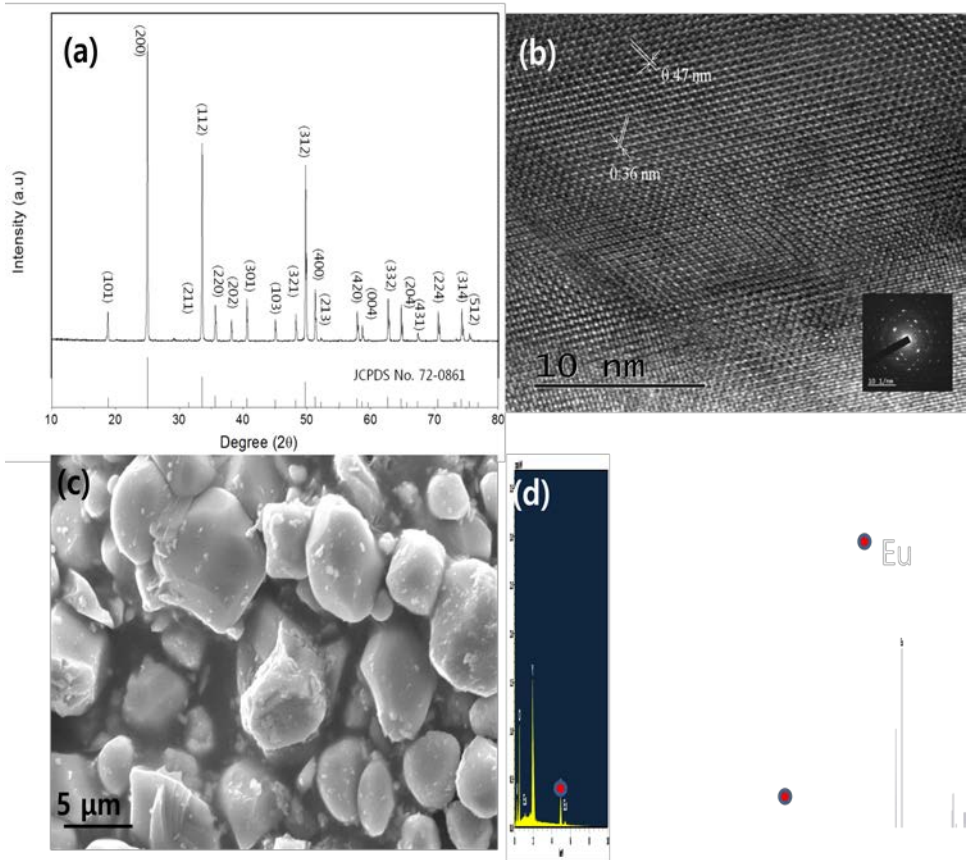


Fig. 2.1 (a) XRD spectra, (b) HRTEM, (c) SEM and (d) EDS spectra of $\text{YVO}_4:\text{Eu}^{3+}$ phosphor synthesized via solid state at 1100 °C.

In this figure it can be seen that solid state synthesized $\text{YVO}_4:\text{Eu}^{3+}$ phosphor is well crystallized almost with no impurity and the XRD pattern is consistent with

JCPDS No. 72-0861. In addition, part (b) shows the significant crystallinity of the synthesized phosphor and the plane distances for two series of (101) and (200) planes have been calculated to be 0.47 and 0.36 nm, respectively. According to SEM image (see Fig. 2.1 (c)), the particles geometry of solid synthesized $\text{YVO}_4: \text{Eu}^{3+}$ phosphor is irregular with the particle size of 4-5 μm . To be sure about the composition of phosphor surface the EDS analysis was done as it was shown in part (d). Accordingly, although the percentage of Eu^{3+} is not very high, but it is observable in the EDS spectra. Also, based on the XRF spectra (not shown) too, the peaks related to Eu^{3+} are observed.

2.3.2. PL Analysis

2.3.2.1. Un-doped YVO₄ phosphor

It has been already shown that un-doped YVO₄ has a luminescence properties too. Guofeng Wang reported a luminescence properties of undoped YVO₄ in the room temperature. Vinit Kumar reported that the broad excitation peak at 320 nm is attributed to the V-O component of VO₄ [18].

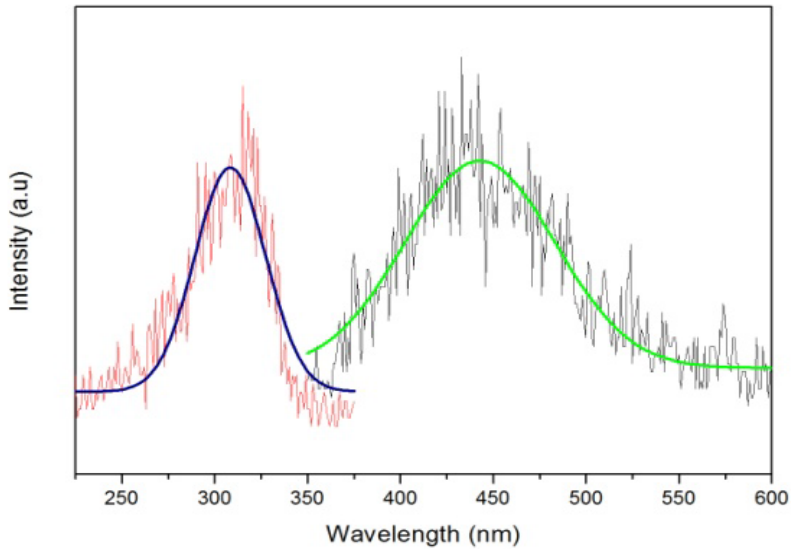


Fig. 2.2 Photoluminescence excitation and emission spectra of combustion synthesized YVO₄ host at the room temperature.

Fig. 2.2 shows the excitation and emission spectra of the un-doped YVO₄ host at the room temperature. From molecular orbital theory, this is attributed to the transitions from ground state 1A_2 (1T_1) to excited states 1A_1 (1E) and 1E (1T_2) of

VO_3^{-4} complexes. A weak line at 396 nm for $\text{Ln} = \text{Eu}$ corresponds to the $^7\text{F}_0 \rightarrow ^5\text{L}_6$ transition of Eu^{3+} . The observed $^7\text{F}_0 \rightarrow ^5\text{L}_6$ transition in the excitation further demonstrates the presence of an energy transfer from VO_3^{-4} groups to Eu^{3+} [19].

2.3.2.2. $\text{YVO}_4: \text{Eu}^{3+}$ phosphor

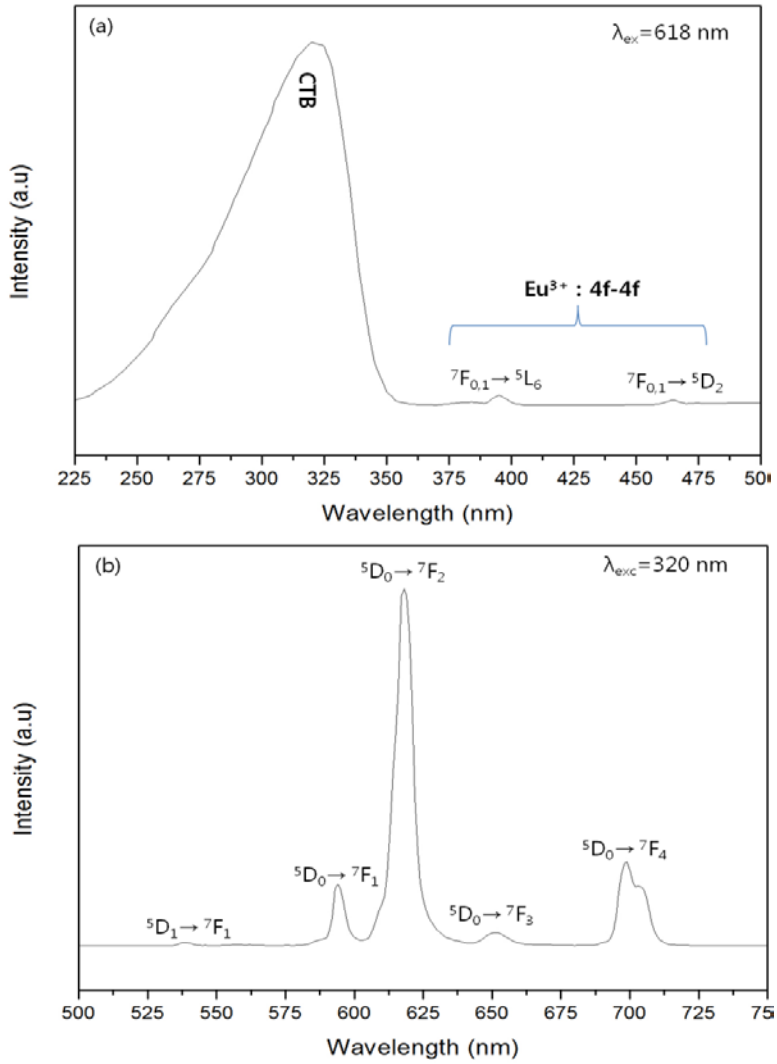


Fig. 2.3 Photoluminescence (a) excitation and (b) emission of $\text{YVO}_4: \text{Eu}^{3+}$ phosphors synthesized via solid state at 1100 °C.

As it is seen in Fig. 2.3 (a), excitation spectrum monitored with 618 nm emission of Eu^{3+} ($^5\text{D}_0$ – $^7\text{F}_2$) consists of a strong and broad excitation band peaked in the region of 250–350 nm. This broad PLE band corresponds to the V^{5+} – O^{2-} metal-to-ligand charge transfer (CT) inside the $[\text{VO}_4]^{3-}$ group [20-23]. The 250 nm excitation band is assigned to the overlap of VO_4^{3-} absorption and charge transfer transition between Eu^{3+} and O^{2-} [24]. Zhou et al. have reported that the VO_4^{3-} absorption in $\text{YVO}_4:\text{Eu}^{3+}$ occurred much more easily than charge transfer of $\text{Eu}^{3+} \rightarrow \text{O}^{2-}$ because of the large differences of charges and ionic radii between V^{5+} (+5, $r = 0.0355$ nm) and Eu^{3+} (+3, $r = 0.107$ nm) [25]. The mentioned main peak with a maximum at about 320 nm is due to the VO_4^{3-} ion. The relatively weak bands from f–f transition lines of Eu^{3+} in the longer wavelength region are observed due to their weak intensity relative to that of the VO_4^{3-} . This indicates that the excitation of Eu^{3+} is mainly through the VO_4^{3-} ions, i.e., by energy transfer from VO_4^{3-} to Eu^{3+} . Excitation into the VO_4^{3-} group at 320 nm yields the emission spectrum (see Fig. 2.3(b)), which not only contains the characteristic transition lines from the lowest excited $^5\text{D}_0$ level of Eu^{3+} but also those from higher energy level ($^5\text{D}_1$) of Eu^{3+} (see Fig.2.4) with a very weak intensity (which can be seen more clearly by enlarging the emission spectrum in the short wavelength region).

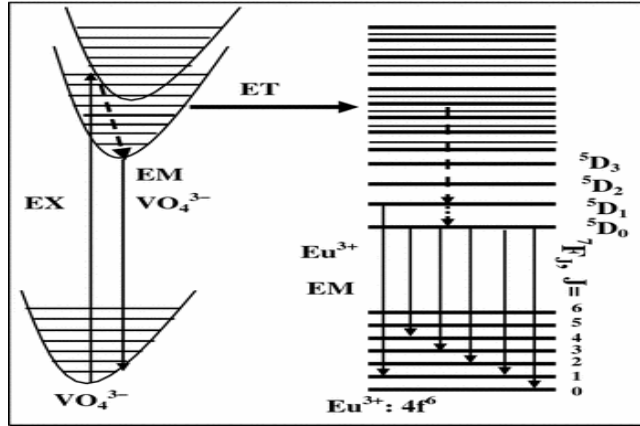


Fig. 2.4 Energy level diagram of Eu^{3+} ions [26].

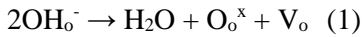
No emission from the VO_4^{3-} group is observed, suggesting that the energy transfer from VO_4^{3-} to Eu^{3+} is very efficient. The locations for the main emission lines of Eu^{3+} and their assignments are labeled in the Fig. 2.3 (b) Obviously, the emission spectrum is dominated by the red $^5D_0-^7F_2$ hypersensitive transition of Eu^{3+} due to the low local symmetry (D_{2d} , without inversion center) for the sites of Eu^{3+} in the YVO_4 host lattices [26]. Note that the $^5D_0-^7F_0$ transition of Eu^{3+} (which is only allowed for C_s, C_n, C_{nv} site symmetry) [27] is absent in the emission spectrum. In addition, the crystal field splitting of $\text{Eu}^{3+}, ^5D_0-^7F_{1, 2, 4}$ transitions, can be seen clearly indicating that the sample is well crystallized. The emission properties of Eu^{3+} are mainly determined by the nearest coordinated VO_4^{3-} ions, whose lower vibration energy (832 cm^{-1}) is not able to bridge the gaps between the higher energy levels and 5D_0 level of Eu^{3+} completely, resulting in the weak emission from these levels.

The number of lines in the emission spectra depends on the symmetry of the Eu^{3+} ion site and results from transitions allowed by the dipole–electric and magnetic rule. The crystal field can influence the $^5\text{D}_0 \rightarrow ^7\text{F}_J$ transition and can split into $2J+1$, depending on the surroundings of the ion. Analysis of the lines in the emission spectra confirmed that symmetry of the Eu^{3+} ion did not depend on the temperature or excitation wavelength. Table 2.1 summarizes the number of observed bands and the maximum charge transfers to the Eu^{3+} ion allowed by the crystal field. The number of bands in the spectrum did not exceed the maximum allowed by the crystal field, demonstrating that the Eu^{3+} ion symmetry was the same in all the samples.

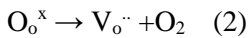
Table 2.1 Number of emission bands for the Eu^{3+} ion

Eu^{3+} ion transitions	Number of bands observed	Maximum amount of allowed " $2J+1$ "
$^5\text{D}_0 \rightarrow ^7\text{F}_0$	1	1
$^5\text{D}_0 \rightarrow ^7\text{F}_1$	2	3
$^5\text{D}_0 \rightarrow ^7\text{F}_2$	4	5
$^5\text{D}_0 \rightarrow ^7\text{F}_3$	5	7
$^5\text{D}_0 \rightarrow ^7\text{F}_4$	2	9

Referring to the literatures related to $\text{YVO}_4:\text{Eu}^{3+}$, the lattice parameters have been calculated to $a = 7.109 (\pm 0.001) \text{ \AA}$ and $c = 6.279 (\pm 0.001) \text{ \AA}$. The change of lattice volume observed for the annealed nano-particles could primarily be due to the increased concentration of oxygen vacancies, though a decrease in the amounts of defect dipoles may also contribute to the slightly reduced lattice volumes [28-29]. Oxygen vacancies in YVO_4 nano-particles might be generated upon dehydration during the annealing process, since the OH^- species anchored to the surface cations will be released, as described by the following Equation:



where OH_o^- , O_o^\times , V_o denote a hydroxy group in the oxygen ion site, oxygen ion on a lattice site, and an oxygen vacancy, respectively. In the YVO_4 lattice, some of the V^{5+} and Y^{3+} ions are threefold (3c) and sevenfold coordinated (7c), respectively. As a result, annealing may result in the formation of oxygen vacancies in the bulk, as well as the reduction of some of the bulk V^{5+} ions in accordance with the following Equation:



Since an oxygen vacancy in the bulk lattice usually has dimensions smaller than that of an oxygen ion, it is highly probable that the occurrence of oxygen

vacancies will give rise to a lattice constriction, different from what we observed for the annealed YVO_4 nanoparticles. This assumption is confirmed by theoretical simulations which show that the YVO_4 lattice volume increases when 0.125 mol of oxygen vacancy is introduced into the bulk lattice. However, the majority of oxygen vacancies could be located at the surfaces of the nanoparticles due to the “self-purified” effect [30]. As a result, oxygen vacancies on surfaces of YVO_4 nanoparticles would strengthen the outward repulsive force imposed on the surfaces causing a slight lattice expansion.

2.3.3. Raman Analysis

Fig.2.5 shows the Raman vibration bands in the range of 100–1000 cm^{-1} . It is well established that for the tetragonal zircon-type YVO_4 with D^{19}_{4h} symmetry (space group $I4_1/amd$), 26 optical modes are possible, which can be expressed by the following irreducible representation [31]:

$$\Gamma = 2A_{1g} + A_{2g} + 4B_{1g} + B_{2g} + 5E_g + A_{1u} + 4A_{2u} + B_{1u} + 2B_{2u} + 5E_u$$

The vibration modes $2A_{1g} + 4B_{1g} + B_{2g} + 5E_g$ are Raman active, and modes $2A_{1g} + B_{2g} + 2B_{1g} + 2E_g$ are related to the internal vibrations of the tetrahedral VO_4^{3-} groups. Therefore, seven vibrational bands observed in the Raman spectra can be assigned accurately, as indicated in Fig. 2.5 Among the observed bands, mode A_{1g} (I) has the highest intensity, while that associated with mode B_{1g} (II) shows the lowest intensity. It can also be seen in Figure that $\text{YVO}_4: \text{Eu}^{3+}$ phosphor after calcination at 900 °C exhibits broad and asymmetrical Raman peaks that become narrow and sharp after calcinations at 1100 °C. Moreover, the symmetry of the peaks increased for the samples after annealing, which indicates the improved crystallinity of the nanoparticles [32].

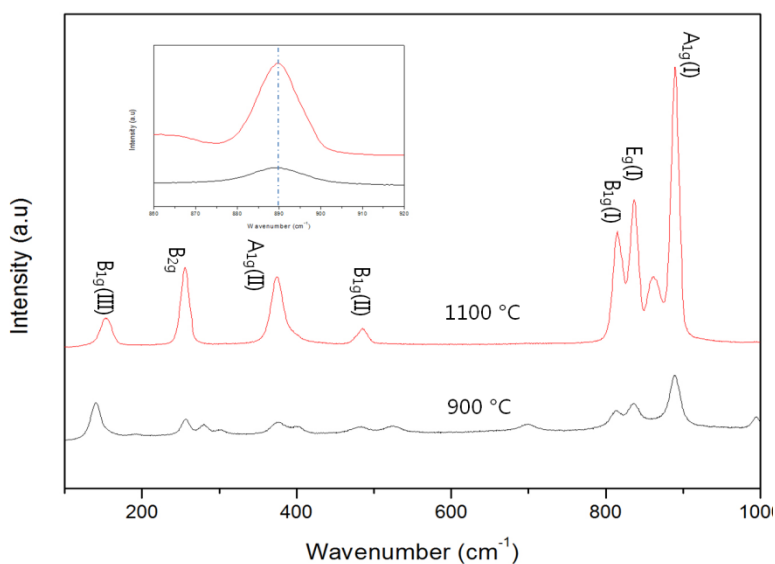


Fig. 2.5 Raman spectra of the $\text{YVO}_4:\text{Eu}^{3+}$ nano-phosphor after calcination at 900 °C and 1000 °C.

The inset of this figure tries to show the asymmetry and symmetry A_{1g} spectra of $\text{YVO}_4:\text{Eu}^{3+}$ phosphor after calcination at 900 °C and 1000 °C, respectively [33].

2.4. Summary and Conclusion

Micron sized $\text{YVO}_4\text{:Eu}^{3+}$ phosphor was synthesized via the simple solid state method in air atmosphere at 1100 °C. Many analyses including XRD, Raman were employed to evaluate the structure and properties of $\text{YVO}_4\text{:Eu}^{3+}$ phosphors. It was found that even un-doped YVO_4 material synthesized in the air atmosphere shows a luminescence property under the excitation wavelength of 310 nm. This behavior of YVO_4 host lattice material is attributed to the formation of many defects. In addition, the $\text{YVO}_4\text{:Eu}^{3+}$ phosphor showed a brilliant red emission with monitoring by the wavelength of 310 nm. Also, the XRD, Raman and HRTEM analysis confirmed the proper crystallinity of solid state synthesized $\text{YVO}_4\text{:Eu}^{3+}$ phosphors. Meanwhile, ESR studies showed that the surface of this phosphor contains a lot of defect. This issue made a motivation to coat the surface of the phosphor by silica.

III. Coating of YVO_4 : Eu^{3+} phosphors with silica

3.1. Introduction

As a host lattice, YVO_4 is known as an excellent material [34-36] especially for rare earth activators it provides the phosphors with noble quantum yields [37-38]. Meanwhile, for the nanometer and submicrometer sized phosphor particles, as it is well known, there are many defects on the surface which can decrease the photoluminescence characteristics. Also, these defects can make the phosphors agglomerated and this issue results in more decrease of luminescence intensity [39]. So, it can be expected to improve the emission properties of phosphor materials by coating of the surface. There are many materials have been known for the coating purpose but among them based on Li et al report, silica and alumina are the most commonly used coating materials While some other materials too have been used as the coating material [44-47]. Furthermore, the related literatures in the fields of phosphor coating show that coating of the surface with SiO_2 usually has been effective to decrease the surface defects [40]. Coating of the phosphors with silica not only is done to decrease the surface defects and enhance the optical properties but also is recommended as an economic point of view. In fact, the rare earth elements are very expensive and then many researchers have tried to design the phosphors in a way to decrease the expenses [48-49]. Noteworthy, phosphors synthesis in the presence of nano

SiO_2 has been introduced since silica is cheap, has a good transparency in the visible region and does not affect the intensity and peak position of PL spectra [50-52]. The physical properties of silica are seen in the appendix. The silica coating can be obtained by a variety of methods including impregnation, precipitation and sol-gel techniques [53-55]. The study about coating of phosphors show that this process for making a relatively uniform coating is a kind of complicated and many parameters affect the coating procedure [56]. It was tried to show some kind of these problems in Fig. 3.1. Different parts of this figure show that in some cases, some parts of phosphor particles are not covered with the coating material and on the other side; there is a kind of coating particles accumulation on some small parts of these particles.

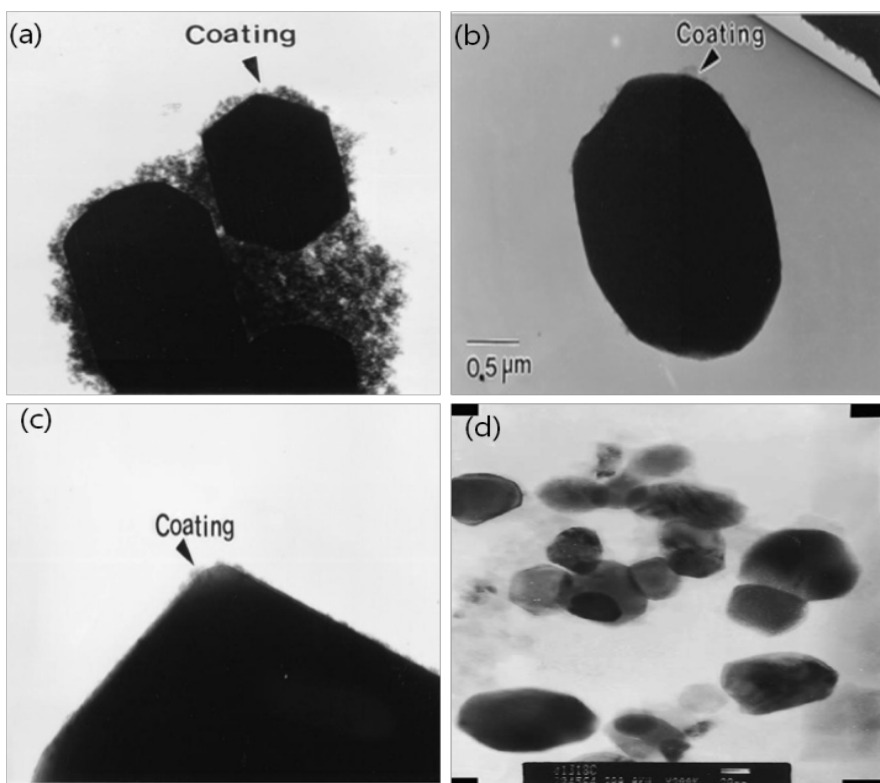


Fig. 3.1 Non uniform coating of SiO_2 on the surface of (a), (b), (c) $\text{Y}_2\text{O}_3\text{:Eu}^{3+}$ and (d) CeO_2 particles.

There are some researches about the silica accompanied phosphor particles via solid state synthesizing at room temperature and spray pyrolysis [57]. Guixia reported silica coated $\text{Y}_2\text{O}_3\text{:Eu}^{3+}$ nano-particles and their luminescence properties where he synthesized these phosphors by a facile solid state reaction method at room temperature [58]. Also, uniform and continuous SiO_2 coating on ZnS phosphor was reported through a sodium silicate by sangdo [59]. In addition,

it has been shown that many phosphors may be degraded in some kinds of corrosive environment and gradually their luminescence properties will be weaker and weaker. Therefore, it can be expected that making a resistant layer of coating on the surface of phosphor particles can improve their stability in the aggressive mediums. Furthermore, since it is well known that Eu^{3+} doped red phosphors have been found to degrade in water-base systems, either by dissolution of the phosphors in the suspension system or by reduction in particle size of the crystallite [60], the formation of a protective silica coating on the surface can be very useful for many applications.

Although it has been reported that SiO_2 coating on the surface of phosphors may potentially enhance the optical performance, but to the best of our knowledge, the application of nano SiO_2 particles for improving the performance of micron sized $\text{YVO}_4:\text{Eu}^{3+}$ phosphors have not yet been reported. In this investigation, the synthesis of a nano layer of silica on $\text{YVO}_4:\text{Eu}^{3+}$ phosphor via sol-gel method was reported. Also, it was shown that the morphology and optical properties of $\text{YVO}_4:\text{Eu}^{3+}$ phosphors depend on many parameters of coating procedure and quantity of coating.

The effective parameters on the morphology of the coating:

SiO₂ does not have any luminescence properties and it is regarded as a dead layer. This layer has two different effects. Firstly it can reduce the reflection of light on the surface followed by absorption increase. Consequently, more portion of excitation light can be absorbed by the phosphor and the photoluminescence properties will be improved. Secondly, there is a kind of penetration loss through incident of the light on the surface. So, in the thick layers of SiO₂ the penetration loss dominates the positive effect of silica. In addition, in the case of making a very thin layer, there is a possibility for incomplete surface coverage. In short, as it was explained in details, for coating of a sample the amounts and the thickness of coating material should be optimum to get a proper optical property.

- Solution pH (7-9 thin coating)

- Temperature

Based on many reports, the amounts of pH and temperature affect the thickness of coating layer on the surface of phosphors [61].

3.4. Experimental

3.4.1. Preparation

3.4.1.1. YVO₄:Eu³⁺ Phosphors Synthesis

To synthesize YVO₄:Eu³⁺ phosphor, analytical grades of yttrium oxide (Y₂O₃), vanadium oxide (V₂O₅), europium oxide (Eu₂O₃) were purchased from Aldrich Company. In a typical procedure, 1 g of yttrium oxide, 0.84 g of vanadium oxide and 0.065 g of europium oxide were mixed and ground by pestle at least for 30 min in a mortar. The obtained powder mixture was synthesized at 1100 °C for 2h in an electrical tube furnace. After calcinations, the mixture was ground again sufficiently.

For the study of the microstructure and photoluminescence characteristics of YVO₄:Eu³⁺ phosphors, SEM and FESEM microscopes, XRD, FTIR, XPS and PL machines were employed.

3.4.1.2. Coating of YVO₄:Eu³⁺ phosphors with silica

The SiO₂-coated YVO₄:Eu³⁺ phosphors were synthesized by the general sol–gel process. The starting materials used in this process were tetraethylorthosilicate (TEOS), NH₄OH, C₂H₅OH with analytic grade purity and de-ionized water. According to the reported synthesis parameters [62] a typical synthesis process was as follows: a mixture of C₂H₅OH (40 ml) and H₂O (8 ml) was prepared in 4 beakers simultaneously followed by addition of 4 ml ammonium hydroxide to be mixed well for 1 h at 60°C. The pH of all these solutions was fixed in the range

of 8-9 by adding proper amounts of citric acid solution. During preparation of the solution, both of temperature and the amounts of pH were under control by a digital and accurate temperature and pH meter. As a typical procedure, 2.5 g of as-prepared $\text{YVO}_4: \text{Eu}^{3+}$ phosphor powders were equally dispersed into the above four beakers, and they were gently stirred at 60 °C for 1 h. Tetraethylorthosilicate (TEOS) in different volume was added into the above 4 beakers under stirring, and the adding amount was 0.5 wt%, 1 wt%, 2 wt% and 4 wt%, respectively, corresponding to the amount of $\text{YVO}_4: \text{Eu}^{3+}$ phosphor. After being stirred for 2 h, these phosphor powders were washed 3 times by ethanol, dried in an oven at 100 °C for 12 h and annealed at 400 °C for 3 h. Finally, SiO_2 -coated $\text{YVO}_4: \text{Eu}^{3+}$ phosphors with various SiO_2 addition content (0.5 wt%, 1 wt%, 2 wt% and 4 wt%) were obtained. For getting these coated phosphors 46.5, 93, 186 and 372 μl TEOS were added, respectively. According to the literatures and as a comparison, the uncoated $\text{YVO}_4: \text{Eu}^{3+}$ phosphor also experienced the same drying process at 100 °C for 12 h and calcination process at 400 and 900 °C for 3 h [43].

3.4.2. Characterization

YVO₄:1%Eu³⁺ phosphors without/ with silica were examined by x-ray diffraction (XRD) with CuK α radiation (λ = 1.54 Å). To study the microstructure of these phosphors, we used scanning electron microscope (SEM) and field emission scanning electron microscope (FESEM). In addition, high resolution transmission electron microscope (HRTEM) was employed to check the structure of synthesized phosphor materials and their crystallinity. Also, the elements and composition of these materials on the surface were measured by x-ray photoelectron spectroscopy (XPS) and for the study of photoluminescence behavior of these phosphors; photoluminescence PL machine (Flip Felix 32) was employed.

3.5. Results and discussion

3.5.1. XRD Analysis

According to the XRD patterns (see Fig.3.2), in all the samples the tetragonal crystal structure, matched with JCPDS No. 72-0861 is seen. In addition, with the addition of SiO₂ no extra peaks related to SiO₂ are observed and we can find that addition of SiO₂ does not make any new phase. This is due to the low amounts of silica and the fact that the formed silica is amorphous and the intensity of this phase is much less than that of strong and well crystallized YVO₄: Eu³⁺ phosphor.

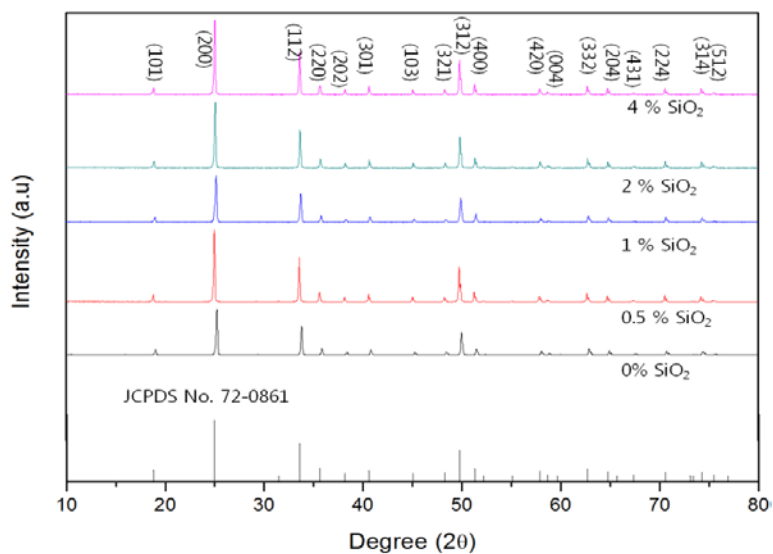


Fig. 3.2 XRD spectra of sol gel synthesized $\text{YVO}_4:\text{Eu}^{3+}$ phosphors with different concentrations of SiO_2 .

3.5.2. FESEM Observations

In Figure 3.3(a), that is related to the bare $\text{YVO}_4:\text{Eu}^{3+}$ phosphor, it is seen that the particle size is about 4-5 μm and it is consistent with the BET analyze that showed the surface area of 0.326 m^2/g for this solid state synthesized phosphor. Also, in parts b, c and d of this figure, that are related to 0.5, 1 and 2 wt% silica, it can be observed that SiO_2 particles are distributed on the surface, homogeneously. The silica particles can be seen in a different color from phosphor particles. In addition, it seems that there is a significant adhesion between silica fine particles and $\text{YVO}_4:\text{Eu}^{3+}$ phosphors. For a better study of silica morphology and particle size the silica colonies were studied by a very high magnification FESEM microscope.

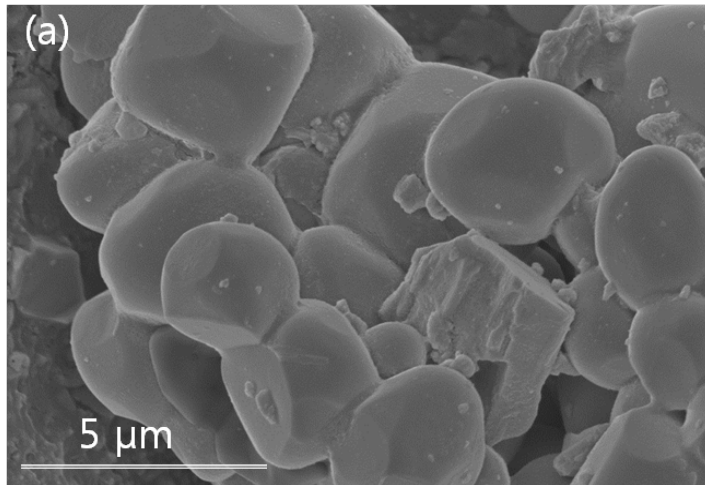


Fig. 3.3(a) FESEM images of bare $\text{YVO}_4:\text{Eu}^{3+}$ phosphors.

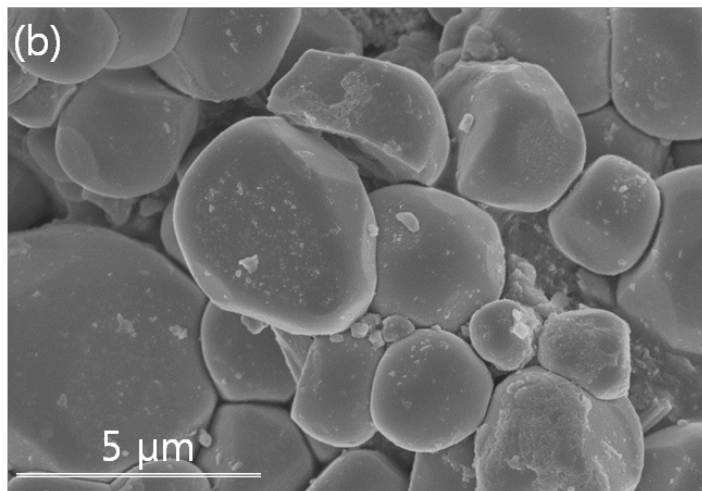


Fig. 3.3(b) FESEM images of $\text{YVO}_4: \text{Eu}^{3+}$ phosphors coated with 0.5 wt% SiO_2 .

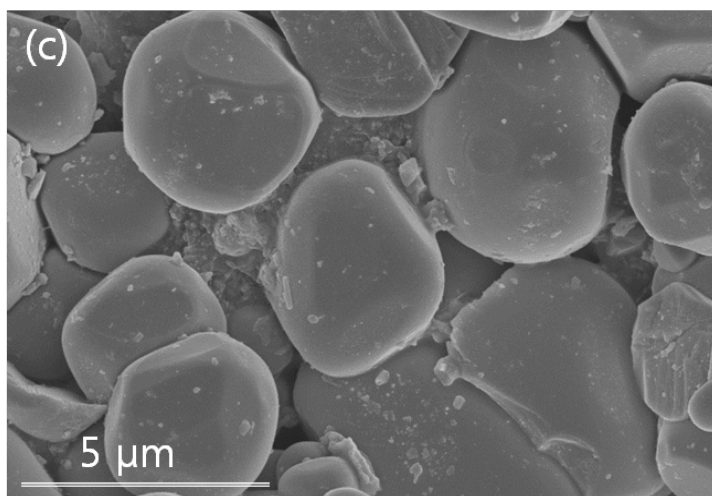


Fig. 3.3(c) FESEM images of $\text{YVO}_4: \text{Eu}^{3+}$ phosphors coated with 1 wt% SiO_2 .

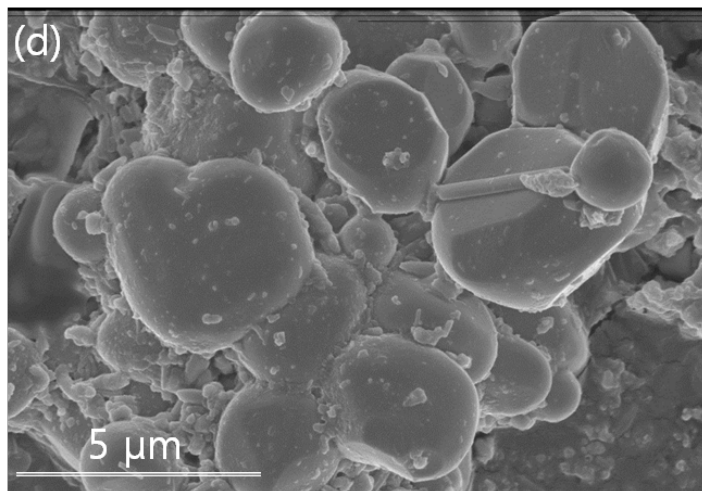


Fig. 3.3(d) FESEM images of $\text{YVO}_4: \text{Eu}^{3+}$ phosphors coated with 2 wt% SiO_2 .

The silica coated $\text{YVO}_4: \text{Eu}^{3+}$ phosphors exhibited the granular microstructure and the surface morphology was almost the same for all of the coated samples regardless of the coating amount. The surface was covered with continuous coating with good adhesion (see Fig. 3.4). As it was shown by high magnification images of FESEM in Fig. 3.4, the formed silica on the surface of phosphors consists of a lot of nano sized particles ranges from approximately 20 to 30 nm. Also, the formation of silica particles on the surface of $\text{YVO}_4: \text{Eu}^{3+}$ particles were confirmed by EDX analysis too (not shown here).

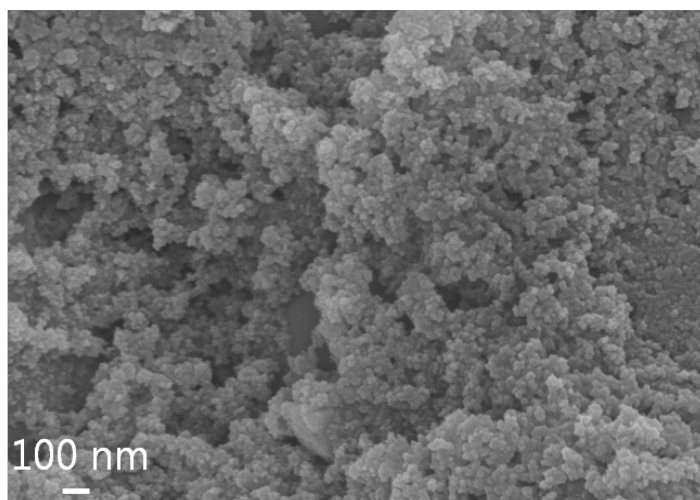


Fig. 3.4 FESEM images of silica coating particles on the surface YVO₄: Eu³⁺ phosphors (in the sample coated with 1 wt% SiO₂).

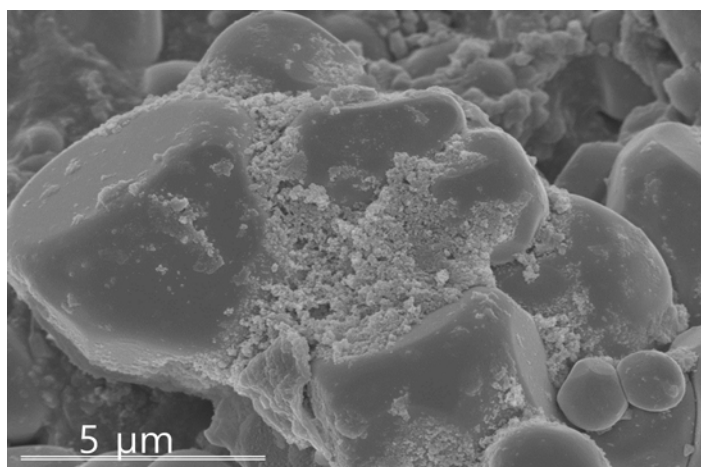


Fig. 3.5 FESEM images of non uniform dispersion of SiO_2 particles in the YVO_4 : Eu^{3+} phosphors coated with 4wt% SiO_2 .

The coating procedure of phosphors with silica is very sensitive to many critical parameters such as temperature, pH, time of stirring that was explained in experimental in detail. Fig. 3.5 shows the FESEM images of the phosphors without any uniform distribution of silica on the phosphor surface. In fact, improper condition of coating procedure can results in a kind of agglomeration of coating particles on the surface.

3.5.3. TEM Observations

To deeper study of the coated silica layer, the surface of the coated phosphors was further analyzed by TEM. Fig. 3.6 shows the HRTEM images of Eu^{3+} doped YVO_4 coated by 1wt% SiO_2 . It is seen that the thickness of coated silica changes mainly from 40 to 60 nm. In addition, the surface of coating layer is very smooth that is a key point for optical properties enhancement [63].

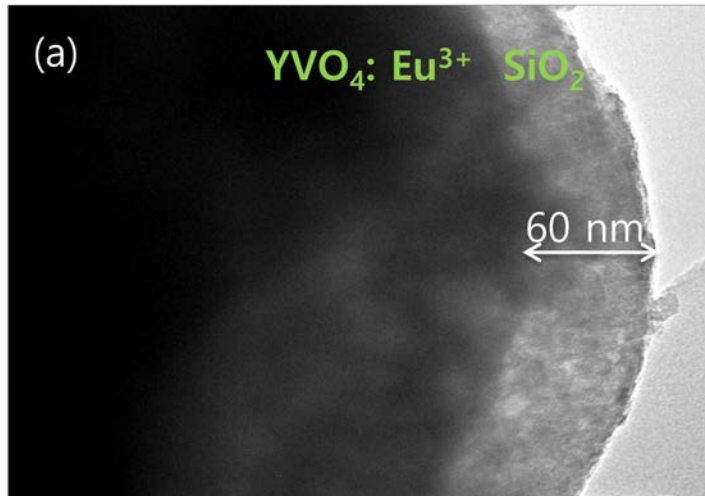


Fig. 3.6(a) TEM images of $\text{YVO}_4: \text{Eu}^{3+}$ phosphors coated with a layer of SiO_2 (1wt% SiO_2).

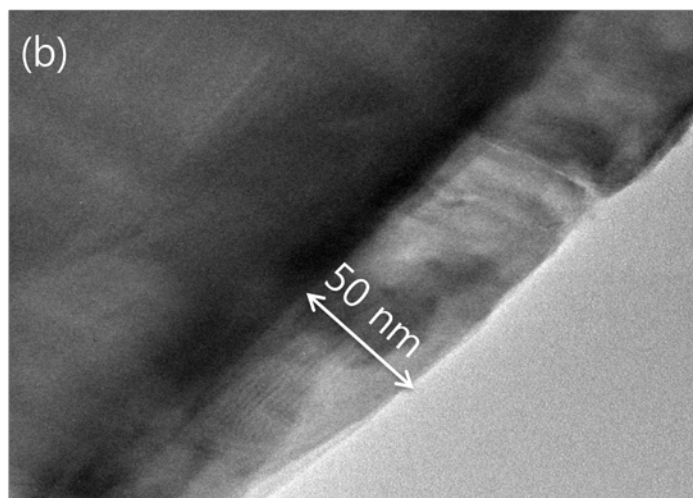


Fig. 3.6(b) TEM images of YVO₄: Eu³⁺ phosphors coated with a layer of SiO₂ (1wt% SiO₂).

In the case of rough coating surface, the scattering phenomena will be very remarkable and the emission intensity of the phosphor is subject to be suppressed seriously. The thickness of coating is a very important parameter since in very thick layers of silica coating on the surface; it acts as a dead zone on the phosphor surface and results in reduction of photoluminescence emission intensity. It is already reported that SiO₂ can be as a barrier for the light emitted from the phosphor. So, the quantity of light escaping from phosphor is reduced [64]. Similar to Fig. 3.5, the agglomeration and non uniform formation of silica particles is shown in Fig. 3.7 by TEM analysis, too. Also, it is concluded that in the improper procedure condition, instead of a smooth and uniform layer of

coating many individual fine particles are formed and a kind of porosity is observed among these particles.

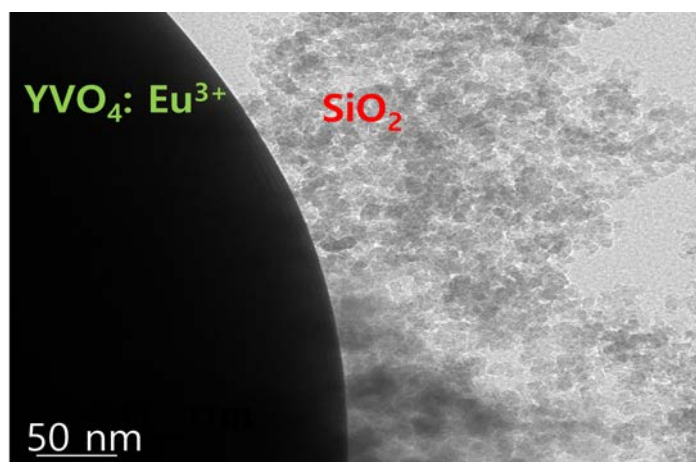


Fig. 3.7 TEM images of non-uniform silica coating on the surface of $\text{YVO}_4: \text{Eu}^{3+}$ phosphors.

3.5.4. XPS Analysis

In order to study the combination of silica coating and $\text{YVO}_4\text{:Eu}^{3+}$ phosphors, the X-ray photoelectron spectra of the uncoated and coated samples were measured. In the Fig. 3.8 the XPS spectra of silica coated $\text{YVO}_4\text{:Eu}^{3+}$ phosphor is shown. In this spectrum the peaks related to O 1s, V 2p, C 1s, Y 3d and Si 2p can be seen as well. The existence of Si 2p peak that is located at 102.72 eV (see Fig. 3.9) in the coated sample, indicate that Silica has been coated on the phosphor particles. The XPS spectra of Y 3d_{5/2} and V 2P & O 1s of the uncoated and coated samples are shown in Fig.3.10 and Fig.3.11, respectively. It can be found that the binding energy of Y 3d_{5/2} for the silica coated samples (158.2 eV) has 1.14 eV chemical shift compared to the uncoated ones (157.06 eV), which infers that silica is likely to be linked with the surface of $\text{YVO}_4\text{:Eu}^{3+}$ phosphors by a Si–O–Y chemical bond. According to the Table 3.1, as the electronegativity of Si is higher than that of Y, the electronic density on the surface of Y is weakened. Therefore, the shielding effect of the surface is weakened and the binding energy of Y 3d_{5/2} is increased [58]. Similarly, it is seen from Fig. 3.11 that the peak position of V 2p in the bare and silica coated $\text{YVO}_4\text{:Eu}^{3+}$ phosphor is 516.66 and 516.77, respectively.

Also, it can be noted that the two peaks of O_{1s} in the bare phosphor are attributed to the surface absorption oxygen located at higher binding energy (about

530.93 eV) and crystal lattice oxygen located at lower binding energy (about 529.42 eV). Similar to the other reports, the intensity of surface oxygen is much larger than that of lattice oxygen. It can be further noted that by silica coating of the phosphors, the intensity of lattice oxygen is lower than that of uncoated one, indicating that the amorphous silica coatings cover the crystal lattice oxygen of $\text{YVO}_4: \text{Eu}^{3+}$ phosphors and then a small portion of the lattice oxygen can be detected in the coated samples. In other words, after the coating process by SiO_2 , the surface oxygen peak will be comparable and close to that of lattice oxygen peak and according to the literatures this peak is attributed to the binding energy for SiO_2 [65]. At the same time, the binding energy of both of oxygen peaks in coated samples has chemical shift to those of uncoated samples, indicating that the silica has been linked on the surface of $\text{YVO}_4: \text{Eu}^{3+}$ phosphors by the chemical bonds. The maximum detectable length of X-ray photoelectron is in nanometer scale, so we can conclude that the silica coating is at nanometer order [58].

Table 3.1 Electronegativity of elements

Elements	Electronegativity
Vanadium	1.63
Yttrium	1.22
Silicon	1.9

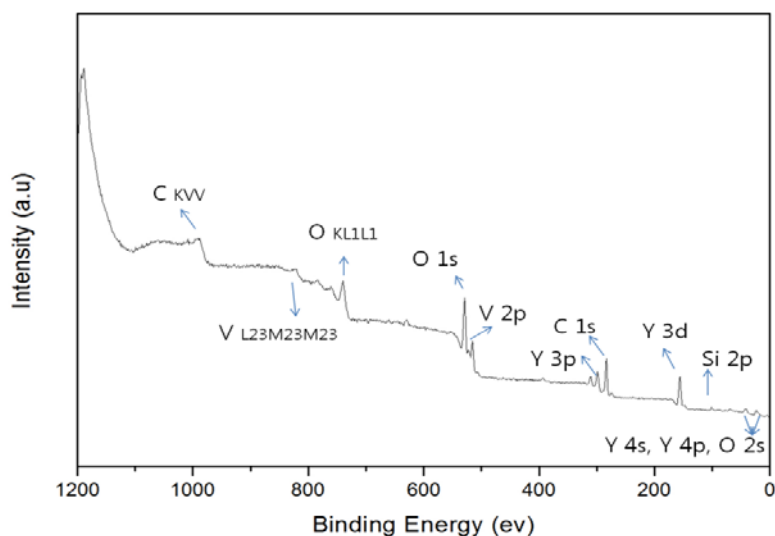


Fig. 3.8 XPS spectra of $\text{YVO}_4: \text{Eu}^{3+}/ 1 \text{ wt\% SiO}_2$ phosphors.

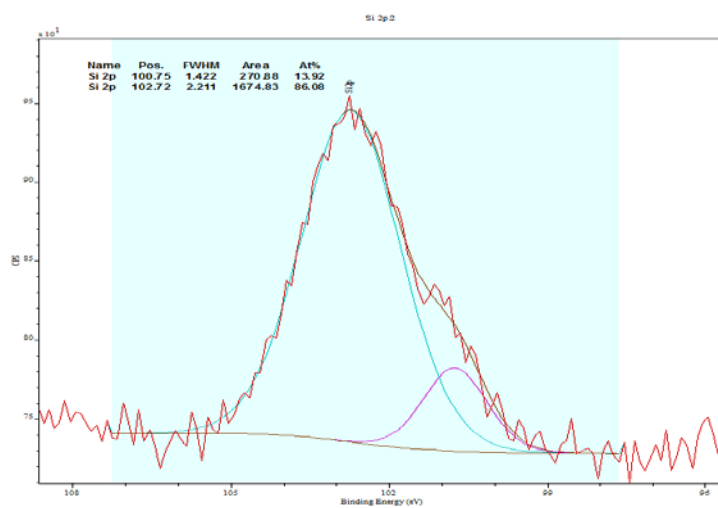


Fig. 3.9 Silicon peaks in the XPS spectra of $\text{YVO}_4: \text{Eu}^{3+}/ 1 \text{ wt\% SiO}_2$ phosphors.

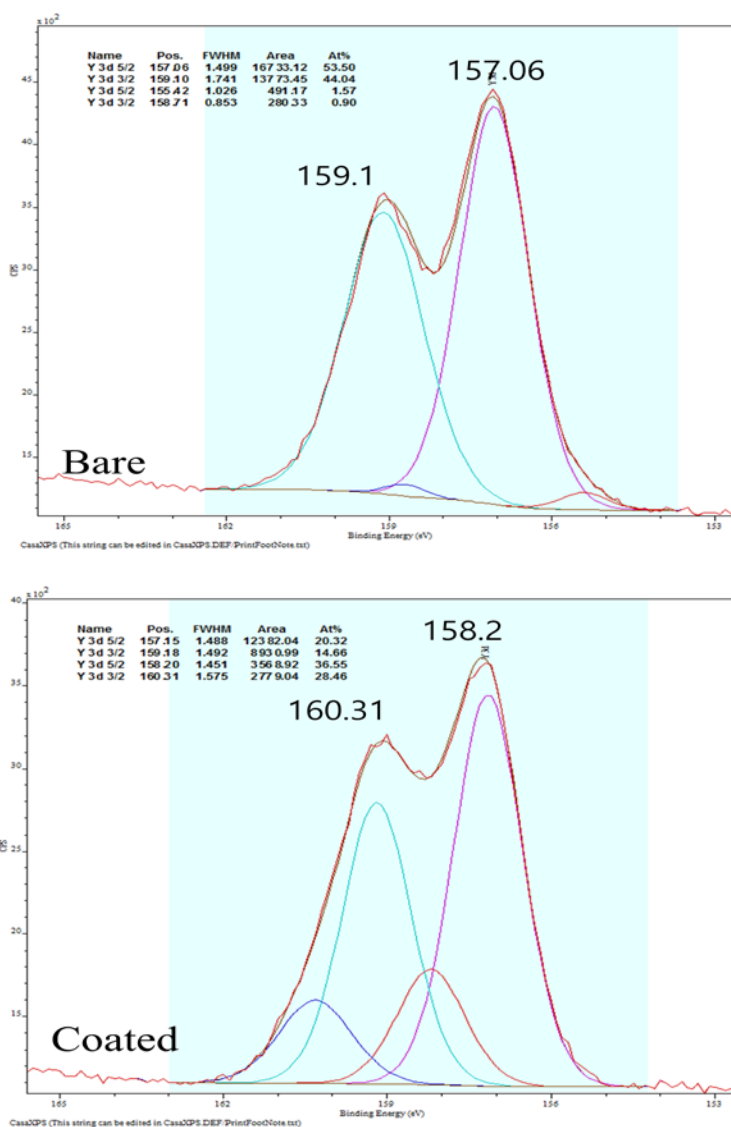


Fig. 3.10 Yttrium peaks in the XPS spectra of bare $\text{YVO}_4\text{:Eu}^{3+}$ and coated $\text{YVO}_4\text{:Eu}^{3+}/1\text{ wt\% SiO}_2$ phosphors.

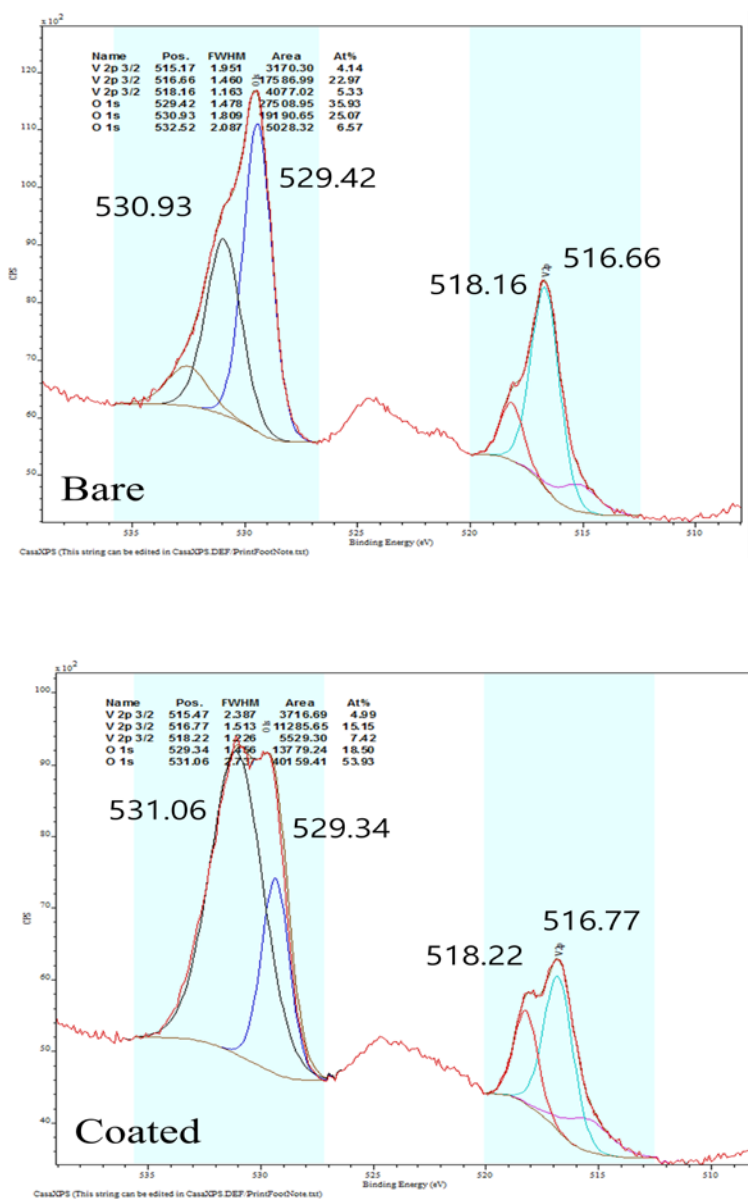


Fig. 3.11 Vanadium and oxygen peaks of $\text{YVO}_4: \text{Eu}^{3+}$ / 1 wt% SiO_2 phosphors.

3.5.5. FT- IR Analysis

The FT-IR spectra of the silica coated $\text{YVO}_4:\text{Eu}^{3+}$ after calcination at 400 and 900 °C with 1 wt% SiO_2 is shown in Fig. 3.12, Fig. 3.13. A strong absorption peak at 824 cm^{-1} and a weak one at 451 cm^{-1} have appeared, which are attributed to the absorption of V–O (from VO_4^{3-} group) and Y(Eu)–O bonds, respectively [66].

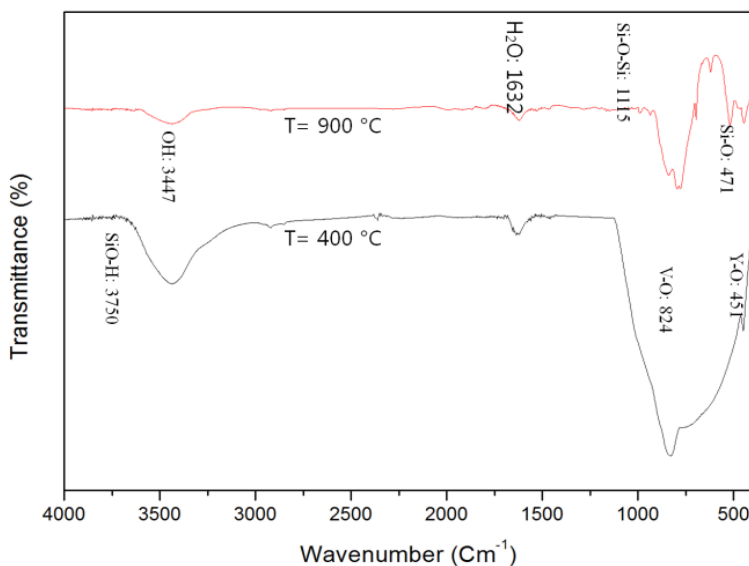


Fig. 3.12 FT-IR spectra of $\text{YVO}_4:\text{Eu}^{3+}$ phosphors with 1 wt% SiO_2 after calcinations at $T = 400\text{ }^{\circ}\text{C}$, $T = 900\text{ }^{\circ}\text{C}$ for 3h.

This suggests that crystalline phase (YVO_4) has formed, agreeing well with the results of XRD [67].

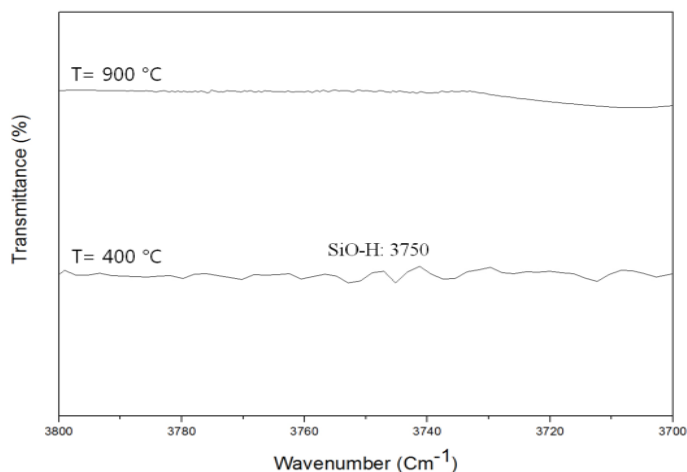


Fig. 3.13 FT-IR spectra of $\text{YVO}_4:\text{Eu}^{3+}$ phosphors with 1 wt% SiO_2 after calcinations at $T= 400\text{ }^\circ\text{C}$, $T= 900\text{ }^\circ\text{C}$ for 3h.

The absorption bands due to OH (3447 cm^{-1}), H_2O (1632 cm^{-1}), Si–O–Si (ν_{as} , 1115 cm^{-1}) and silanol or SiO–H (3750 cm^{-1}) are observed [68]. This indicates that the as-formed SiO_2 particles contain a large amount of OH groups and H_2O on their surfaces [69]. The surface SiO–H groups which is well known as a luminescence quencher is going to be diminished with the increase of post calcinations temperature. In addition, the strength of Si–O–Si absorption band is increasing with post heating of the coated phosphor.

3.5.6. PL Analysis

Referring to Fig.3.14, excitation spectrum monitored with 618 nm emission of Eu^{3+} ($^5\text{D}_0 \rightarrow ^7\text{F}_2$) consists of a strong and broad excitation band with a maximum at about 320 nm due to the VO_4^{3-} ion.

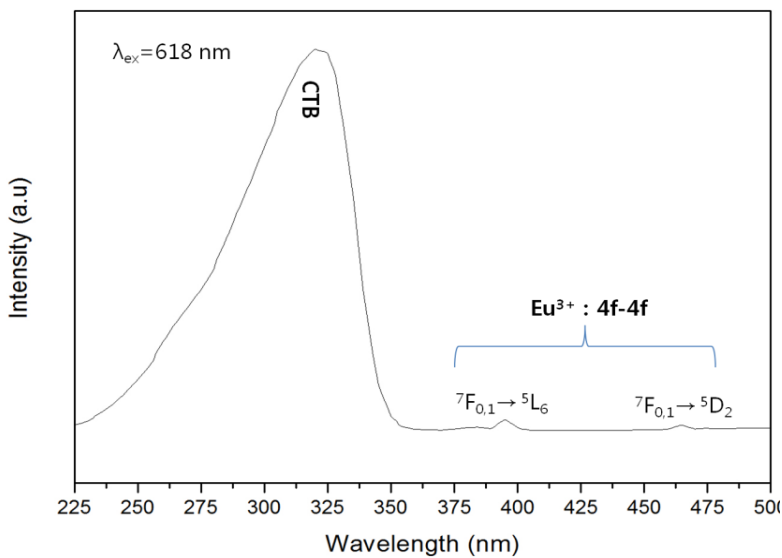


Fig. 3.14 Photoluminescence excitation of $\text{YVO}_4:\text{Eu}^{3+}$ phosphor.

The relatively weak bands from f-f transition lines of Eu^{3+} in the longer wavelength region are observed due to their weak intensity relative to that of the VO_4^{3-} . In the emission spectrum (see Fig. 3.15), no emission from the VO_4^{3-} group is observed, suggesting that the energy transfer from VO_4^{3-} to Eu^{3+} is very efficient.

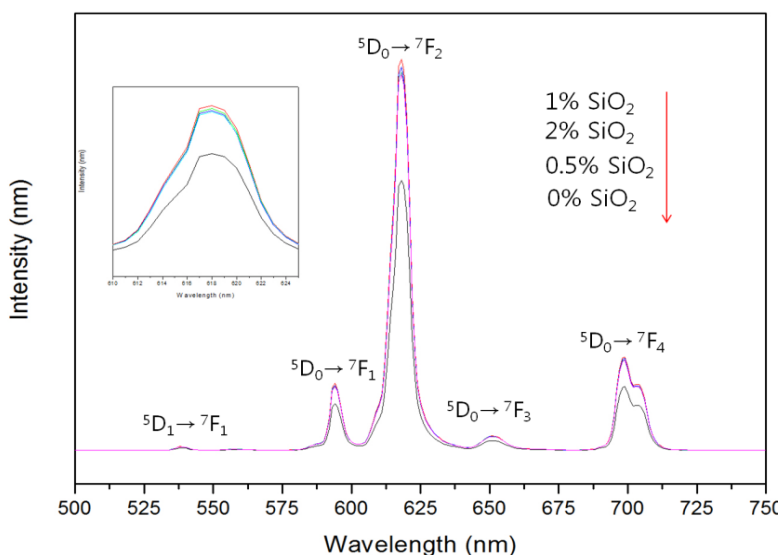


Fig. 3.15 Photoluminescence emission spectra YVO₄: Eu phosphors with different concentrations of SiO₂.

In addition, it is seen that the maximum emission intensity is related to the coated phosphor with 1 wt% SiO₂. The locations for the main emission lines of Eu³⁺ and their assignments are labeled in the Fig. 3.15 which confirms that the emission spectrum is dominated by the red $^5D_0 \rightarrow ^7F_2$ hypersensitive transition of Eu³⁺ in the YVO₄ host lattices. Generally, in the silicate host lattices with high phonon energy (at about 1100 cm⁻¹ for the vibration frequency of Si–O–Si bond), it has been reported that the emission from the higher energy levels (5D_1 , 5D_2 , 5D_3) of Eu³⁺ is quenched completely by the multi-phonon relaxation process [70]. However according to Fig. 3.15, in YVO₄:Eu³⁺ phosphors coated with SiO₂, the

emission from higher excited states of Eu^{3+} is present despite the high-energy phonons of Si–O–Si from the SiO_2 cores (1114 cm^{-1} , Fig. 3.11). This indicates that the SiO_2 coating layer has little influence on the luminescence properties of the phosphors due to the long distance of between Si–O–Si networks and the Eu^{3+} ions. The emission properties of Eu^{3+} are mainly determined by the nearest coordinated VO_4^{3-} ions, whose lower vibration energy (832 cm^{-1}) is not able to bridge the gaps between the higher energy levels and $^5\text{D}_0$ level of Eu^{3+} completely, resulting in the weak emission from these levels. All the above spectral properties for the $\text{YVO}_4:\text{Eu}^{3+}/\text{SiO}_2$ phosphors are basically consistent with the reported bulk [71-72] nano-crystalline powder [73] and thin film [67,74].

3.5.6.1. Reflection

To study the mechanism of luminescence enhancement of the silica coated $\text{YVO}_4:\text{Eu}^{3+}$ phosphors, a schematic view of the phosphor particles has been shown in Fig. 3.16. By considering the type and composition of the material and based on the interface zone among the three components (phosphor- SiO_2 -phosphor), the total refracted light from the material (r_{tot}) under light-scattering conditions is approximately as below:

$$r_{\text{tot}} = r_1 + r_2 \cdot \exp(-i \cdot \Psi_d) / 1 + r_1 \cdot r_2 \cdot \exp(-i \cdot \Psi_d) \quad (1)$$

Where r_1 and r_2 are the amplitude refraction coefficients at the interfaces of medium 2, (in the front and back surfaces of medium 2, respectively. Also, i is the imaginary constant ($i=\sqrt{-1}$)), and ψ_d is the phase difference between the incident and refracted light.

$$r_{tot}=r_1[1-\exp(\theta)] \text{ where } (\theta = -i.\psi_d) \quad (2)$$

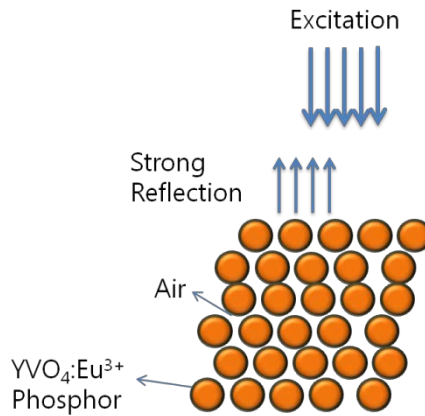


Fig. 3.16 Strong reflection of bared $\text{YVO}_4:\text{Eu}^{3+}$ phosphors under excitation.

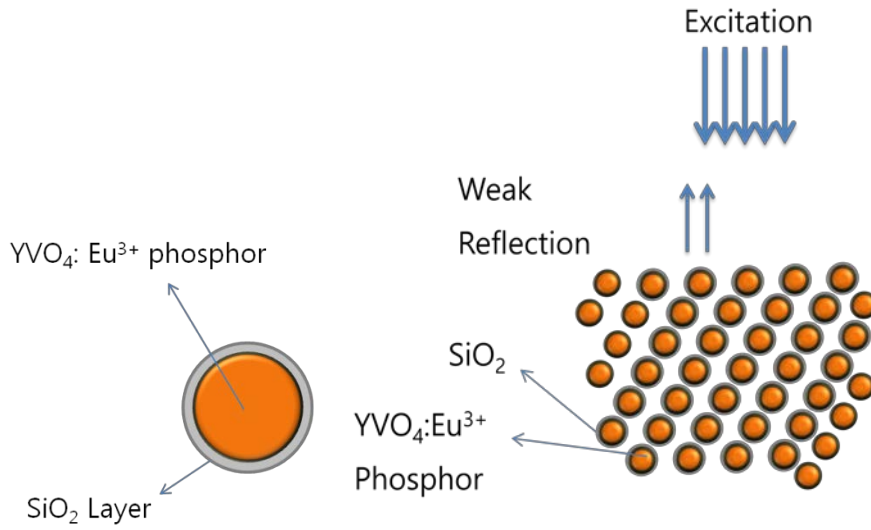


Fig. 3.17 Weak reflection of bared $\text{YVO}_4:\text{Eu}^{3+}$ phosphors under excitation.

Then it can be found that:

$$r_{\text{tot}} = \frac{n_1 - n_2}{n_1 + n_2} [1 - \exp(-\theta)] \quad (3)$$

The power reflection coefficient R of a material can be found from the ratio of the sum of the intensities of electromagnetic waves refracted from the front and back surfaces to the intensity of the incident electromagnetic wave:

$$R = r_{\text{tot}}^2 = \left(\frac{n_1 - n_2}{n_1 + n_2} [1 - \exp(-\theta)] \right)^2 \quad (4)$$

Less reflection coefficient (R) results in the higher absorption of the excitation energy. As a result, the excitation energy can be sufficiently incorporated into the phosphor material. Assuming that θ has the same value for the YVO_4 samples with and without added SiO_2 , the reflection coefficient (R) values are as follows. In the absence of SiO_2 , since air is present among the particles (see Fig. 3.16), and the refractive indexes of YVO_4 and air that are 2.006 and 1, respectively, the value of $R_{\text{YVO}_4/\text{Air}}$ is $0.112 \alpha^2$, where $\alpha = [1 - \exp(-\theta)]$.

In the case of the YVO_4 : Eu/ SiO_2 materials (see Fig. 3.17), the reflection coefficient ($R_{\text{YAG}/\text{SiO}_2}$) can be calculated from the ratio of the refractive indexes of YVO_4 and SiO_2 . Using the refractive index of SiO_2 of 1.45, the value of $R_{\text{YVO}_4/\text{SiO}_2}$ was $0.026 \alpha^2$, which is approximately 0.23 that of $R_{\text{YVO}_4/\text{Air}}$. This calculation shows that the SiO_2 in the YVO_4 structures played a crucial role in the inhibition of the scattering of exciting light. In the cases of low R values, sufficient exciting light can reach the inside of the phosphor particles, as indicated in Fig. 3.16.

3.5.6.2. Quantum Yield

Considering the reflectance of the phosphor powder samples at an excitation wavelength, the QE of phosphors can be calculated as follows [75- 78]:

$$\%QE = \text{Number of emitted photons} / \text{Number of excited photons} * 100$$

The number of emitted photons is considered to be proportional to the integrated intensity of the PL emission. And the number of absorbed photons is considered to be proportional to the intensity of the excitation radiation (after reflectance correction), one more effect by the SiO₂ coating on the deposit's optical property can be found in the absorption and external and internal quantum efficiencies (QE) of the two deposits with and without the SiO₂ coating, as exhibited in Table 3.2 as a function of the excitation wavelength. The internal (η_{in}) and external (η_{ex}) efficiencies were calculated using the following equations:

$$\eta_{ex} = (\int \lambda \cdot P(\lambda) d\lambda) / (\int \lambda \cdot E(\lambda) d\lambda)$$

$$\eta_{in} = (\int \lambda \cdot P(\lambda) d\lambda) / (\int \lambda (E(\lambda) - R(\lambda)) d\lambda)$$

Where $E(\lambda)/h\nu$, $R(\lambda)/h\nu$, and $P(\lambda)/h\nu$ are the numbers of photons in the excitation, reflectance, and emission spectra of the phosphor, respectively [79]. Under the 320 nm excitation, the internal efficiency in the uncoated phosphors is 67 %, while it is increased to 77.9 % in the case of coated phosphors. This is similar to the research done by D. Cervantes that showed the silica coating of Y₂SiO₅: Ce,Tb phosphor enhance the efficiency about 12% [76].

Table 3.2 The quantum efficiencies for bare and coated YVO₄:4%Eu³⁺

Sample	λ_{exc}	λ_{em}	IQE
YVO ₄ :4%Eu	310	617.95	0.67
YVO ₄ :4%Eu /1 wt%SiO ₂	310	617.95	0.779

3.5.7. Chemical Stability

3.5.7.1. Water Degradation

Many phosphors including $\text{YVO}_4:\text{Eu}^{3+}$ one are widely used in fluorescent lamps as a source of red light. During fabrication of fluorescent lamps, a suspension of phosphor material in an aqueous system may be used.

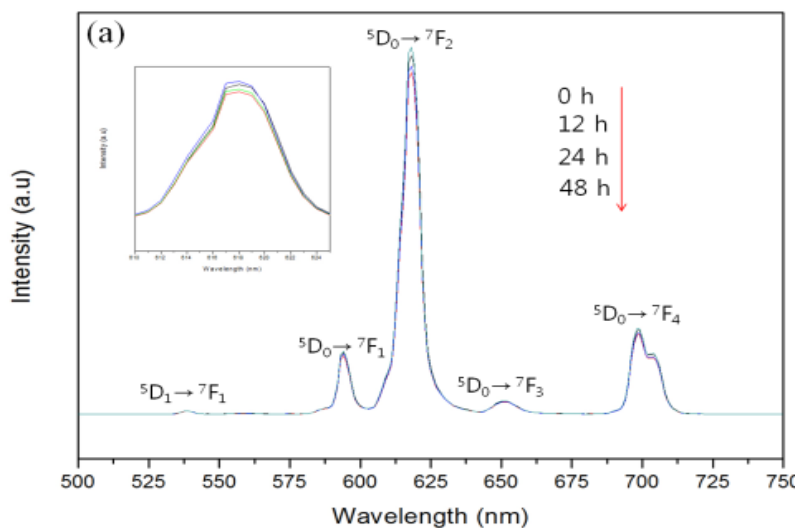


Fig. 3.18(a) Photoluminescence emission spectra of bare $\text{YVO}_4:\text{Eu}^{3+}$ phosphors after different times of immersion in water.

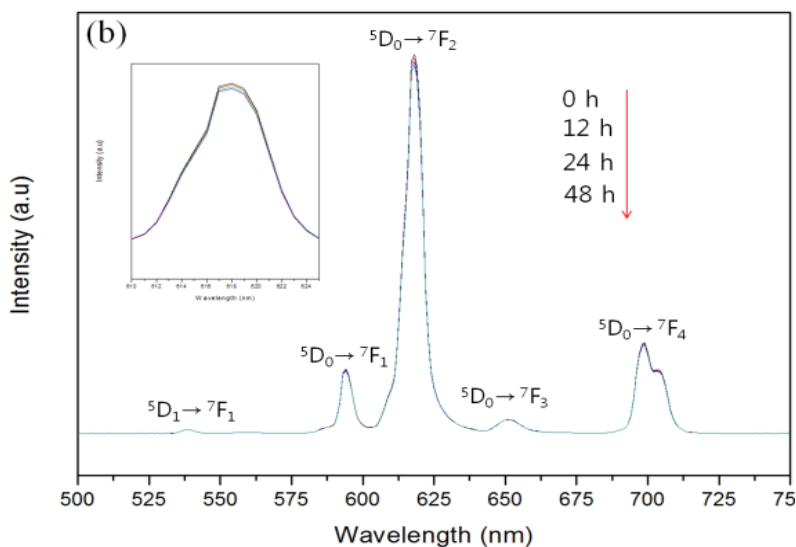


Fig. 3.18(b) Photoluminescence emission spectra of $\text{YVO}_4: \text{Eu}^{3+}$ phosphors with 1 wt% SiO_2 after different times of immersion in water.

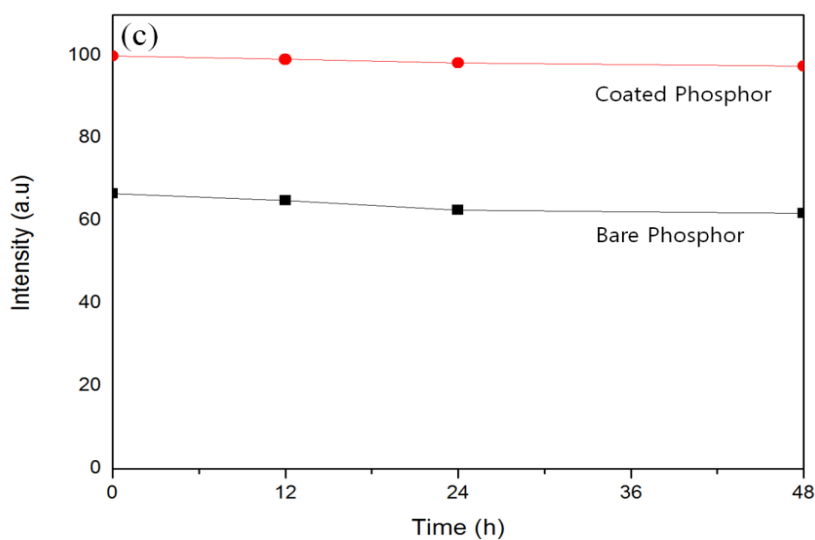


Fig. 3.18(c) Photoluminescence emission spectra of $\text{YVO}_4: \text{Eu}^{3+}$ phosphors without and with 1 wt% SiO_2 after different times of immersion in water.

On the other side, the degradation of phosphors in the aqueous media due to their solubility or breakup of crystallite, makes some limitations in phosphors application. Specially, Eu^{3+} doped red phosphors have been found to degrade in water-base systems, either by dissolution of the phosphors in the suspension systems or by reduction in particle size of the crystallite [80]. To see the degradation behavior of these phosphors, after coating of the surface of phosphors with 1 wt% SiO_2 , the coated phosphors were immersed in water for different times of 12, 24 and 48 h, individually. We prepared 3 samples (every sample was 2 g) of 1 wt% SiO_2 -coated phosphors and immersed them in 50 ml de-ionized water for different times in 3 beakers, individually. Also, for getting a reference, this part was repeated exactly for 3 bare phosphors. Then the samples were separated from the water, dried and then used to measure their PL properties. Fig.3.18 shows the PL spectra of bare and coated phosphors after different soaking times in water. As shown in this Figure, there is no remarkable difference among the peak positions of PL spectra of SiO_2 -coated and uncoated samples. For better study of the PL spectra of these phosphors, the insets of this figure indicate the PL intensities, in higher magnification. The reduction rate of the emission intensities for the coated samples is smaller than those of the uncoated samples after they were immersed in water at the same time. The results (see Fig. 3.18 (b)) of these experiments clarify that the intensities of emission spectra of coated samples decreased more slightly than that of the bare

samples (see Fig. 3.18 (a)) with the increasing immersing time. According to what was explained, it can be found that the moisture-resistance stability of SiO_2 -coated $\text{YVO}_4:\text{Eu}^{3+}$ phosphor was improved to a large extent, although the quantity of added SiO_2 was not remarkable in the coating procedure of $\text{YVO}_4:\text{Eu}^{3+}$ phosphor.

3.5.7.2. Acid Degradation

Recent studies show that $\text{YVO}_4:\text{Eu}^{3+}$ has significant promise in plasma display panels (PDP) [81]. Recently, LnVO_4 ($\text{Ln} = \text{Y}, \text{La}, \text{Gd}$ and Lu) materials have attracted much attention in PDP applications due to their high thermal and chemical stability and high luminescence efficiency under VUV excitation [82]. Also, for the phosphors used in PDP industries chemical stability is one of the critical properties [83].

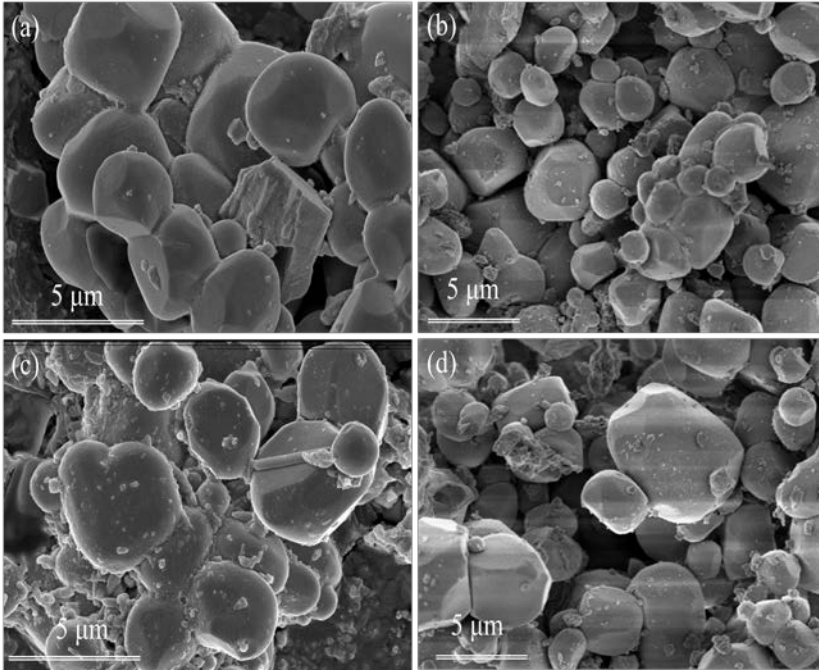


Fig. 3.19 FESEM images of $\text{YVO}_4:\text{Eu}$ phosphors with (a), (b) 0 wt% SiO_2 , (c), (d) 2 wt% SiO_2 , before and after immersing in acid for 15 min.

As an specific procedure, 0.25 g uncoated and 0.25 g of 1 wt% SiO_2 -coated phosphors into two series of beakers filled with of HNO_3 (1 ml of 95% acid) and HCl (8.5 of 35% acid) and then 15 ml of de-ionized water was added to all of

beakers at the same time. Accordingly, after the immersion in the mixture of acid for 15 min, it was followed by separation through centrifuge at the speed of 3000 rpm for 5 min. The acid was analyzed by ICP to measure the amounts of dissolved elements and the remained powders were washed by de ionized water 3 times. Table 3.3 shows the ICP data of both coated and uncoated phosphors and it is obvious that coating of phosphors with silica somehow prohibits the dissolution of these phosphors. In other words, the concentration of Y, V and Eu in acid is higher in the case of bare phosphors than those of coated one. For example the amounts of Yttrium elements of bare $\text{YVO}_4:\text{Eu}^{3+}$ phosphor is 102.11 ppm in the acid solution while it reduced to 82.35 and 63.17 for $\text{YVO}_4:\text{Eu}^{3+}\text{-2\%SiO}_2$ and $\text{YVO}_4:\text{Eu}^{3+}\text{-4\%SiO}_2$ phosphors, respectively. This data shows the protection of phosphor particles in aggressive mediums very well.

Table 3.3 the amounts of elements (ppm) of bare and coated $\text{YVO}_4:4\%\text{Eu}^{3+}$ phosphors in the acid mixture solution.

Composition	Y	V	Eu	Si
$\text{YVO}_4:\text{Eu}$	102.11	96.67	8.34	-
$\text{YVO}_4:\text{Eu-2\%SiO}_2$	82.35	57.7	6.08	7.54
$\text{YVO}_4:\text{Eu-4\%SiO}_2$	63.17	44.77	4.77	12.07

Also, the morphology of collected phosphor powders was studied by the FESEM right after drying at 100 °C. Fig. 3.19 Shows the FESEM morphology of the bare and coated phosphors before and after immersion in the mixture of acid. It is seen that bare phosphors have been solved partially in acid media since the particle size has decreased from 4.3 μm to 3.5 μm , approximately. Conversely, we cannot see a remarkable difference between the size of coated phosphor particles before and after soaking in the acid mixture. This result is consistent with the explained ICP data and is an indirect influence of SiO_2 coating on the properties of phosphor particles.

3.5.8. Thermal quenching

In the white LEDs application, the temperature dependence of phosphor is important because it has great influence on the light output and color-rendering index [84]. The temperature of the substrate of LED lamps usually increases to 100–150 °C and even higher for street lamps, because heat is produced continuously during LED operation. The thermal stability of LED luminescence depends strongly on phosphors [85].

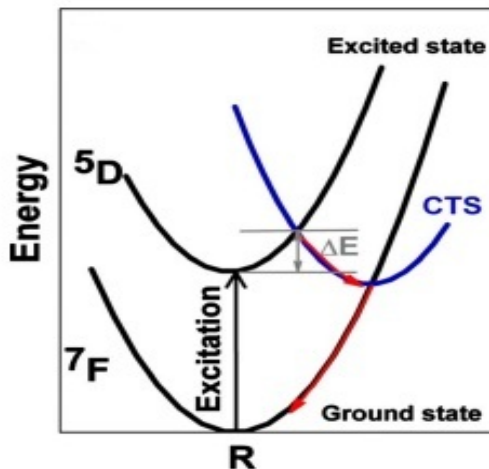


Fig. 3.20 Schematic of charge transfer between ground and excited states.

It is known that the luminescent ion can reach the ground state via thermal quenching. In other words, it can reach the ground state when the excited state and the ground state energy curves cross at an energy which is thermally

accessible from the relaxed excited state (see Fig.3.20). The activation energy of bare phosphor is smaller than that of coated one, indicating that the coating of SiO_2 on the surface of phosphor increase the thermal resistant and suppress the thermal quenching [86].

Fig. 3.21 clearly shows that coating the phosphor with SiO_2 decrease the thermal quenching effect. In fact for the bare $\text{YVO}_4:\text{Eu}^{3+}$ phosphors, the intensity of $^5\text{D}_0\text{-}^7\text{F}_2$ peak reduced about 12% when the temperature increased from 25 to 175°C .

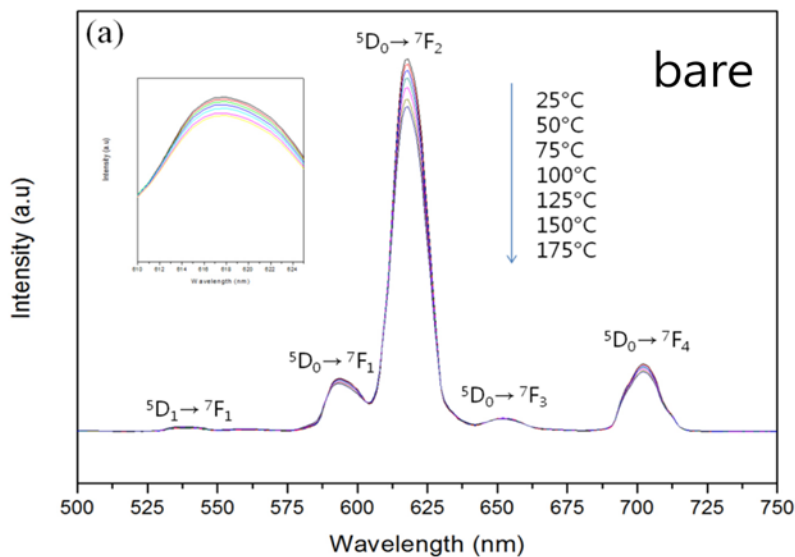


Fig. 3.21(a) Temperature dependent Photoluminescence emission spectra of bare $\text{YVO}_4:\text{Eu}^{3+}$ phosphors.

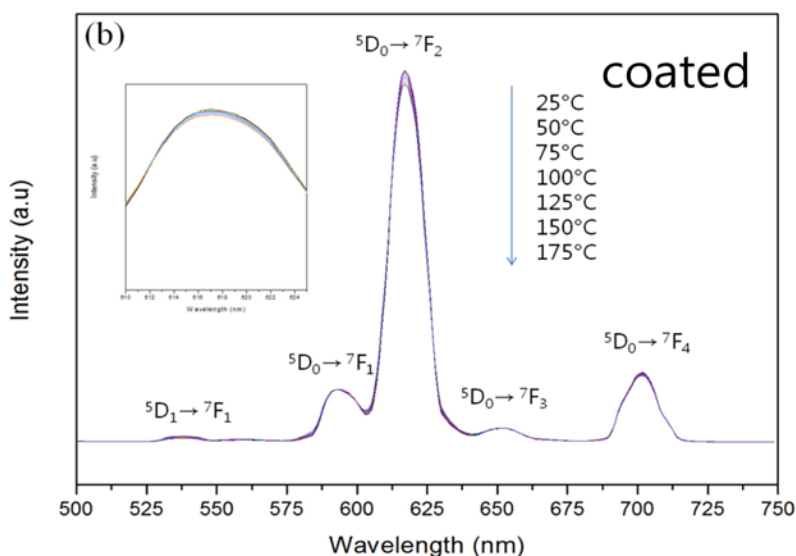


Fig. 3.21(b) Temperature dependent Photoluminescence emission spectra of $\text{YVO}_4:\text{Eu}^{3+}$ phosphors with 1 wt% SiO_2 .

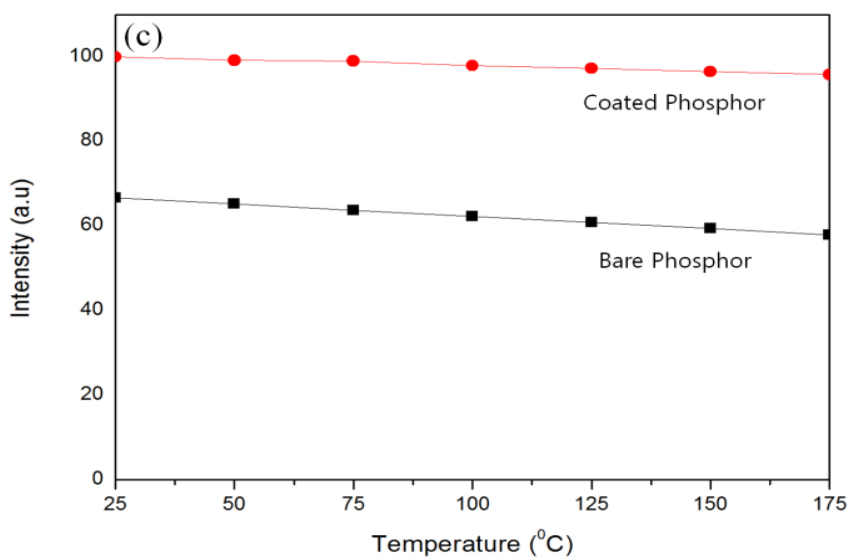


Fig. 3.21(c) Temperature dependent Photoluminescence emission spectra of $\text{YVO}_4:\text{Eu}^{3+}$ phosphors without and with 1 wt% SiO_2 .

In summarize, the results indicate that the value of T50 for these phosphors is above 175°C, indicating that these phosphors have good thermal stability; the thermal stability of coated phosphor is superior to that of bare phosphor.

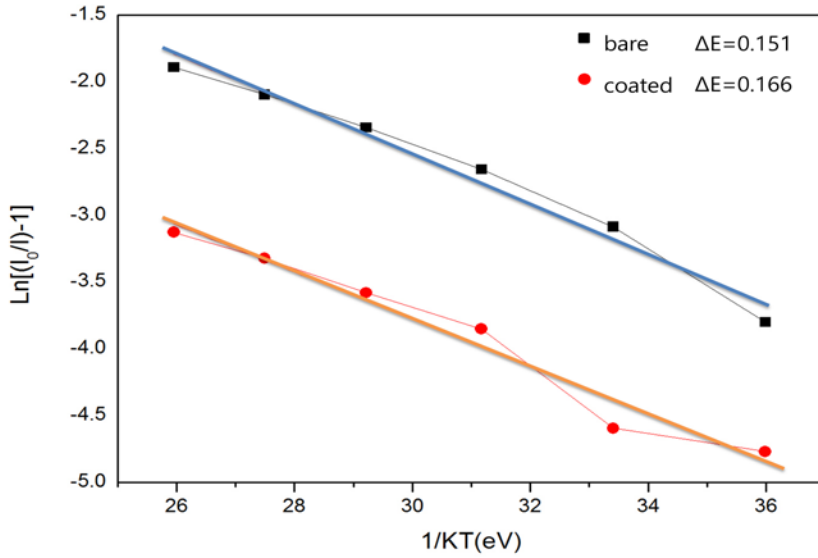


Fig.3.22 Activation energy for the thermal quenching process in the YVO₄: Eu³⁺ phosphors without and with SiO₂.

It is known that the luminescent ion can reach the relaxation state via thermal quenching. In other words, it can approach to the ground state while the excited state and the ground state energy curves cross at an energy which is thermally accessible from the relaxed excited state. It is assumed that the non-radiative rate (k_{nr}) can be expressed as follows [87- 88]:

$$k_{nr}=A\exp(-\Delta E/kT)$$

Where A is a constant, k is Boltzmann's constant, and ΔE is the activation energy for the thermal quenching process. Thus, the emission intensity decreases due to the probability of non-radiative transition increasing with temperature. According to the above equation, a lower value of ΔE means a more rapid non-radiative rate at a given temperature. Noteworthy, higher amounts of ΔE is a sign of higher resistant for thermal quenching process. The Arrhenius equation can be used to describe the temperature dependence of the luminescent intensity.

$$I(T)=I_0[1+C\exp(-\Delta E/kT)]$$

Where I_0 is the initial intensity, $I(T)$ is the intensity at given temperature T according to Kelvin degree, C is a constant, k is Boltzmann's constant, and ΔE is the activation energy for the thermal quenching process, was fitted to the thermal quenching data. The activation energy of thermal quenching can be estimated from the slope of the $\ln\{[I_0/I(T)]-1\}$ vs $1/kT$ plot. As shown in Fig. 3.22, the activation energies of $YVO_4: Eu^{3+}$ and $YVO_4: Eu^{3+}$ coated with 1wt% silica for the thermal quenching process is 0.151 and 0.166 eV, respectively. The thermal quenching of the emission intensity of $YVO_4: Eu^{3+}$ activated phosphors at higher temperatures is due to the excited electrons easily jumping into the CTS band after absorbing thermal energy, at which the probability of non-radiative

transition may increase. Thus, the emission intensity of Eu^{3+} activated phosphors decreases with increasing temperature. The activation energy of $\text{YVO}_4:\text{Eu}^{3+}$ is smaller than that of silica coated one, indicating that the former is more sensitive to the thermal effect.

3.5.9. ESR Analysis

Fig.3.23 shows the Electron Spin Resonance (ESR) spectra of $\text{YVO}_4:\text{Eu}^{3+}$ phosphors in the cases of bare and coated with 1wt% SiO_2 . The bare phosphor shows two main peaks that is related to V^{4+} while the coated phosphor indicates almost a flat line without any significant peak. Vanadium with the atomic number of 23 has the electron configuration of $4s^2 3d^3$. Then V^{5+} is paired while the V^{4+} ion is unpaired (has a single electron) and we can detect the V^{4+} ions easily by ESR analysis. Meanwhile, one of the common reported defects in YVO_4 based phosphors is V^{4+} that is because of oxygen vacancies. It is clear that the valence change of V ions could be closely related to the annealing at relatively low oxygen partial pressure. As a conclusion, calcination atmospheres have significant influences on the lattice defect structure of $\text{YVO}_4:\text{Eu}^{3+}$ phosphors and the defect structures would play an important role in luminescence performance [17,89].

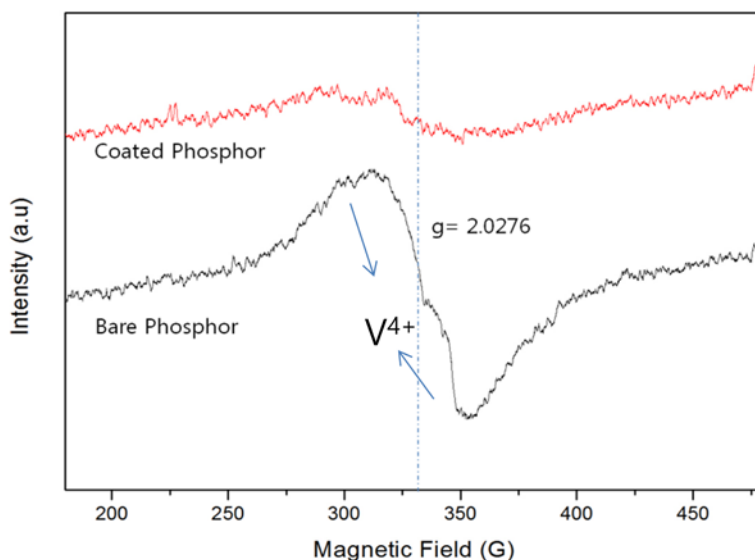


Fig. 3.23 ESR spectra of $\text{YVO}_4:\text{Eu}^{3+}$ phosphors in the cases of bare and coated with 1 wt% SiO_2 .

Liusai reported that under oxygen atmosphere, EPR signals of V^{4+} ions were greatly decreased and almost disappeared and furthermore, when the precursor was pretreated under air or even nitrogen atmospheres at 800°C for 2 h, hyperfine structures and much intensive defect signals for lower oxidation state vanadium ion (+4 or even +3) in distorted tetragonal structure appeared, indicating a higher concentration of defects [17].

3.6. Summary and Conclusion

In this investigation, it was found that coating of $\text{YVO}_4:\text{Eu}^{3+}$ phosphors by silica layers increased the emission intensity due to reduction of reflection and decrease of surface defects. To study about the surface defects, the ESR analysis was employed and a significant decrease of surface defects after coating with silica was confirmed. The maximum photoluminescence emission intensity of the coated phosphors with an adhered and smooth coating with the thickness of 40-60 nm occurred at 1 wt% SiO_2 . From the chemical shift of O_{1s} , $\text{Y}_{3d\ 5/2}$ and $\text{V}_{2p\ 3/2}$ peaks in XPS, it is concluded that SiO_2 is coated on the surface of phosphors. Also, based on the FT-IR studies, vibrations of O-Si-O and Si-OH are found to be 1115 and 3750 cm^{-1} , respectively. Interestingly, with increasing annealing temperature, peak intensity of Si-OH decreases whereas that of O-Si-O increases. This suggests that samples heated at lower temperature show the presence of silanol group which acts as a luminescence quencher.

Noteworthy, the silica coating of $\text{YVO}_4:\text{Eu}^{3+}$ phosphors not only enhanced the photoluminescence properties but also improved the resistant in thermal quenching too. It was found that even coating of the phosphors with 1 wt% SiO_2 results in a significant resistant of thermal quenching. Furthermore, since T50 of the silica coated $\text{YVO}_4:\text{Eu}^{3+}$ phosphors is more than 175 °C, many applications specially in the field of LED, can be considered for this phosphor.

IV. Core shell $\text{YVO}_4\text{:Eu}^{3+}\text{@SiO}_2$ phosphors

4.1 Introduction

Recently, the typical spherical core-shell structured phosphors have been interestingly studied based on their significant and potential applications in photonic crystals, catalyst and biological labelling [91-94]. For the core-shell structured phosphor materials, the structure, size and composition can be easily designed in a controllable way to get the favourite properties of these materials [95]. The ideal morphology for phosphor particles includes a perfect spherical shape, narrow size distribution, and non-agglomeration. Spherical morphology of the phosphors is an ideal shape of phosphor particles for high brightness and high resolution. Additionally, high packing densities and low scattering of light can also be obtained by using spherical phosphors [96]. So far, many synthetic methods have been developed and modified to control the size and distribution of phosphor particles, such as spray pyrolysis [97] and urea homogeneous precipitation [98]. As a host material used for laser oscillation, YVO_4 is easy to handle and has a strong birefringence that ensures the polarization state of emitted light. Eu^{3+} activated YVO_4 is an important commercial red phosphor used in color television, the cathode ray tube (CRT) and the high-pressure mercury lamp, which was reported first by Levine and Palilla [71,99]. Thus, a great deal of research work has been fulfilled to the procedure development for the synthesis of $\text{YVO}_4\text{:Eu}^{3+}$ particles of varied sizes in a controllable manner. Among them, core shell synthesis has been known as a promising and effective

method to produce uniform and spherical shaped phosphors. If the silica spheres are coated with phosphor layers, a kind of core-shell phosphor material with spherical morphology will be obtained and the size of the phosphor particles can be controlled by the silica cores. Furthermore, because silica is much cheaper than most of the phosphor materials, specially the phosphors which employ expensive rare-earth elements as activators, the cost of core-shell phosphor materials become much more cheaper and economic than the pure phosphor materials. Recently, several investigators have reported on the deposition of nanoparticle phosphors on silica spheres. In this investigation, by a modified synthesis, the spherical and monodisperse silica particles (which size ranges from 350-450 nm) were produced and then the surface was coated with layers of $\text{Y}_{0.96}\text{Eu}_{0.04}\text{VO}_4$ phosphor via a citrate sol-gel process [100]. The advantages of this method include the easy control of the morphology of the final phosphor particles by silica cores and lowering the cost of the final phosphors due to the partial substitution of cheaper SiO_2 for the expensive materials. In addition, the effect of LiCl addition to the phosphor shells was studied as well.

4.2. Experimental

4.2.1. Synthesis of silica cores

Amorphous spheres of silica in the size range of 350–450 nm were synthesized by hydrolysis of tetraethyl orthosilicate (TEOS) in ethanol medium in the presence of water and ammonia by a modified procedure of the well-known Stöber method (Stöber et al. 1968). In this method the colloidal solution of silica particles with a narrow size distribution in the sub-micrometer range, and the particle size of silica depended on relative concentration of the reactants. In a typical experiment, 10.5 ml of TEOS, 4.5 ml of de-ionized H₂O, and 122.5 ml of NH₄OH were added into 112.5 ml of ethanol and stirred at room temperature for 4 h, resulting in the formation of white silica colloidal suspension. The silica particles were centrifugally separated from the suspension and washed with ethanol for four times.

4.2.2. Synthesis of SiO₂@Y_{0.96}Eu_{0.04}VO₄ core–shell phosphors

SiO₂–core Y_{0.96}Eu_{0.04}VO₄–shell particles (SiO₂@Y_{0.95}Eu_{0.05}VO₄) were prepared by a sol–gel process. The starting materials were Y₂O₃ (1g), Eu₂O₃ (0.065 g), NH₄VO₃ (1.08 g), and citrate acid as the additive. The detailed procedure was as follows: First the mentioned stoichiometric weights of oxide were dissolved in dilute nitric acid, and corresponding nitrate solutions were obtained. Then

certain amount of citric acid, the molar ratio of which to total metal cation was 6:1, was added into mixed nitrate solution as chelating agent for the metal ions. The pH of the solution was adjusted to 6 with ammonium hydroxide followed by the addition of stoichiometric amount of NH_4VO_3 , and then the silica particles were added under stirring. This procedure has been shown in Fig.4.1. The suspension was continuously stirred at 80 °C for several hours until it turned to sticky blue sol, and the sol was dried at 100 °C for 24 h to obtain the blue gel. The powders were calcined at 900 °C for 3 h to obtain the $\text{SiO}_2@Y_{0.96}\text{Eu}_{0.04}\text{VO}_4$ core-shell phosphors

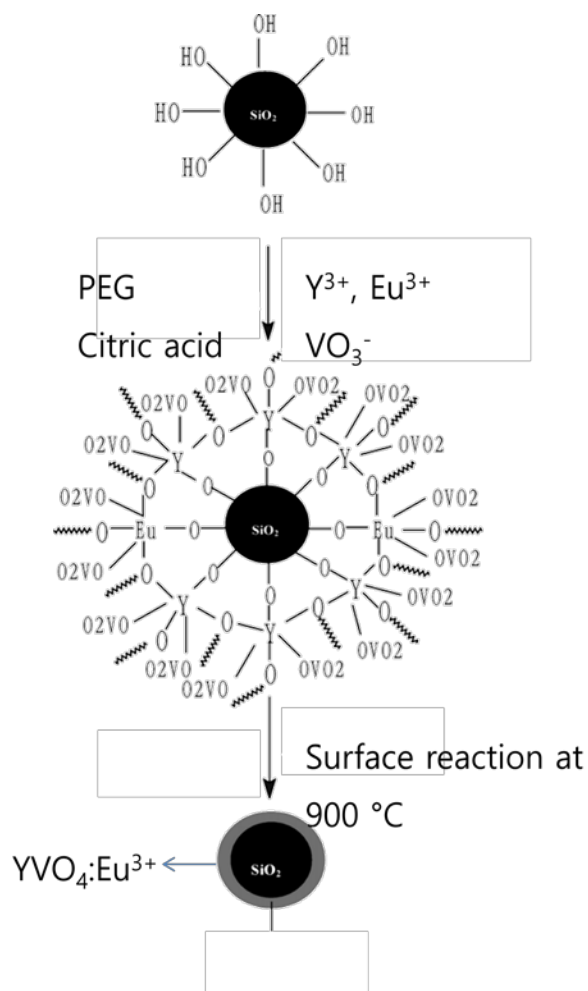


Fig. 4.1 Schematic view of core-shell procedure for $\text{SiO}_2@Y_{0.96}Eu_{0.04}VO_4$ phosphors

4.3. Results and discussion

4.3.1.XRD Analysis

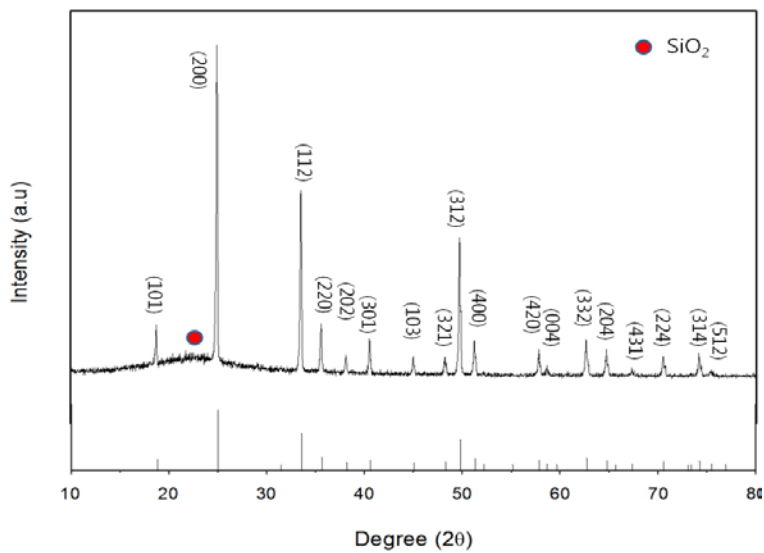


Fig. 4.2(a) XRD spectra of Core shell $\text{YVO}_4:\text{Eu}^{3+}@\text{SiO}_2$ phosphors.

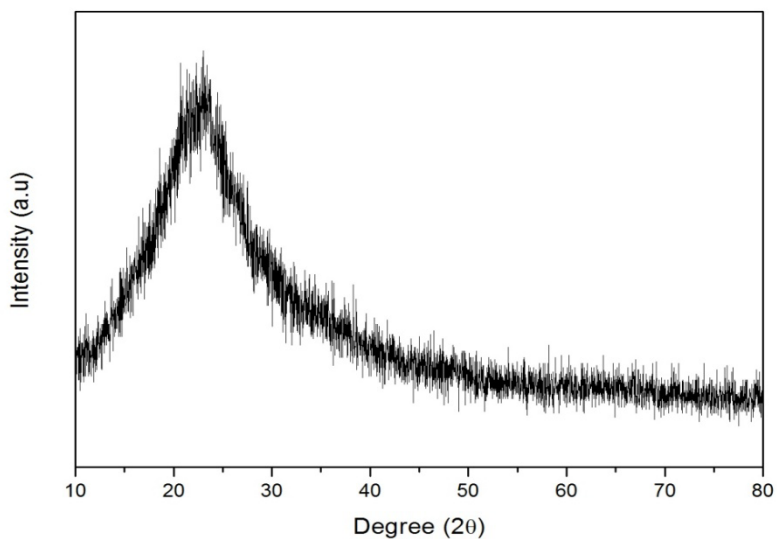


Fig. 4.2(b) XRD spectra of SiO_2 core.

The XRD spectra of 900 °C calcined $\text{SiO}_2@Y_{0.96}\text{Eu}_{0.04}\text{VO}_4$ core shell phosphor is shown in Fig. 4.2(a). Referring to this result, the pattern is well matched with the JCPDS card No. 76-0861 for YVO_4 . Also, no diffraction peak is observed except for a very broad band centered at approximately $2\theta=22.00^\circ$, which is the characteristic peak for amorphous SiO_2 (JCPDS 29-0085). The XRD spectrum of as-formed fresh SiO_2 (without any calcination) is shown in Fig. 4.2 (b). It can be seen that the synthesized silica does not have any crystallinity. For the $\text{SiO}_2@Y_{0.96}\text{Eu}_{0.04}\text{VO}_4$ core-shell sample besides the broad band of SiO_2 that was explained former, all the diffraction peaks belonging to crystalline YVO_4 are present, suggesting that the coatings of $\text{Y}_{0.96}\text{Eu}_{0.04}\text{VO}_4$ have been crystallized well on the surfaces of amorphous silica particles. This is in good agreement with the situation for the pure $\text{YVO}_4\text{:Eu}^{3+}$ powder sample. In addition, it is very important to notice that no other phase or impurity can be detected in the XRD spectra which show the perfect synthesis of $\text{SiO}_2@Y_{0.96}\text{Eu}_{0.04}\text{VO}_4$ core-shell phosphors.

4.3.2. FESEM Observations

Fig. 4.3 shows the FESEM micrographs of the as formed SiO_2 particles, pure $\text{YVO}_4:\text{Eu}^{3+}$ powders, $\text{YVO}_4:\text{Eu}^{3+}@\text{SiO}_2$ core shell phosphors by three layers

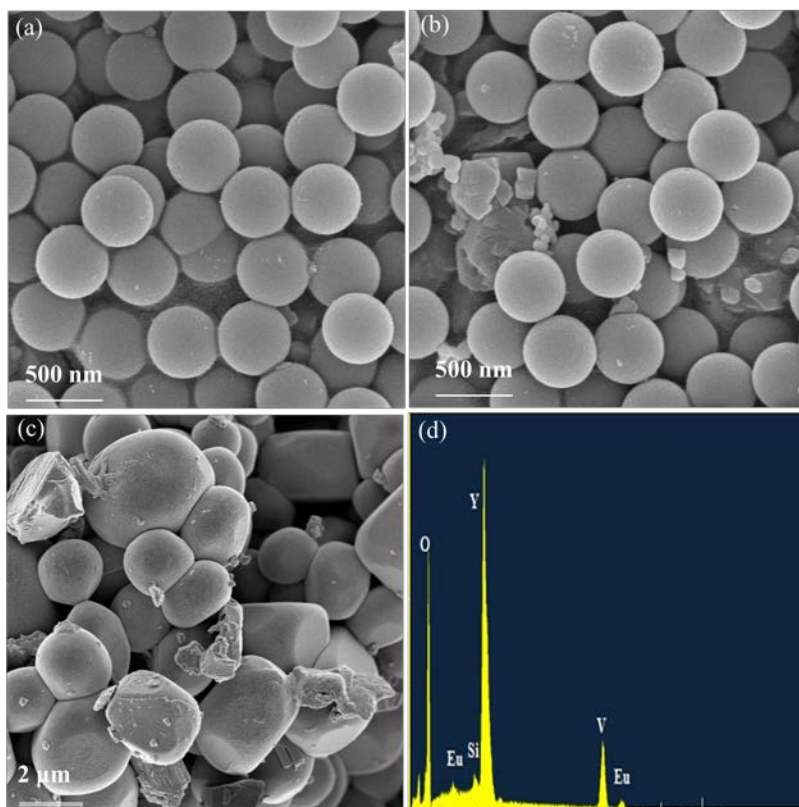


Fig. 4.3 FESEM image of (a) SiO_2 core, (b) Core shell $\text{YVO}_4:\text{Eu}^{3+}@\text{SiO}_2$, (c) $\text{YVO}_4:\text{Eu}^{3+}$ phosphors and (d) EDX of $\text{YVO}_4:\text{Eu}^{3+}@\text{SiO}_2$ core shell phosphors.

of $\text{YVO}_4:\text{Eu}^{3+}$ and EDX spectra of $\text{YVO}_4:\text{Eu}^{3+}@\text{SiO}_2$ core shell phosphors that are observed in parts a-d of this figure, respectively. From the Fig. 4.3 (a), it is seen that the as formed SiO_2 consists of spherical particles with an average size

of about 400 nm, and noteworthy in these particles almost no aggregation has been made with a narrow size distribution. After completing the specific core shell synthesis on SiO_2 cores that was explained in details in the experimental part, the resulted $\text{SiO}_2@ \text{YVO}_4:\text{Eu}^{3+}$ particles still keep the spherical morphology of the silica particles, and still no agglomeration can be found in the FESEM image (see Fig.4.3(b)). Maybe the main difference of $\text{SiO}_2@ \text{YVO}_4:\text{Eu}^{3+}$ particles with the synthesized SiO_2 core particles is that the size of the core shell phosphor is slightly larger than the pure silica particles due to the addition of $\text{YVO}_4:\text{Eu}^{3+}$ layers on amorphous silica particles. To see better the effect of core/shell procedure on the morphology of phosphors, the FESEM image of pure $\text{YVO}_4:\text{Eu}^{3+}$ powders synthesized through sol-gel procedure was shown in Fig.4.3(c). It is obvious that many aggregated particles are seen in this material and the particle size is not uniform and changes from 1.5 to 4 μm . In addition, the morphology of the pure $\text{YVO}_4:\text{Eu}^{3+}$ phosphor is irregular while that of core/shell phosphor was spherical. Part d of Fig. 4.3 that was obtained with the energy-dispersive X-ray analysis, shows that the composition of the surface of $\text{SiO}_2@ \text{YVO}_4:\text{Eu}^{3+}$ core shell particles is composed of Si, O, Y, Eu and V elements. This data is well matched with XRD spectrum of the core shell phosphor and shows that $\text{YVO}_4:\text{Eu}^{3+}$ layer is well formed on the amorphous silica cores. However, it should be mentioned that the FESEM micrographs can only provide the basic information on the morphology of phosphor particles in large scale and the core-shell structure of $\text{SiO}_2@ \text{Y}_{0.96}\text{Eu}_{0.04}\text{VO}_4$ particles cannot

be confirmed and resolved from the FESEM micrographs based on the limitations of magnification.

4.3.3. HRTEM Observations

In order to evaluate the core-shell structure of $\text{SiO}_2@Y_{0.96}\text{Eu}_{0.04}\text{VO}_4$ phosphors more accurately, the HRTEM analysis was employed.

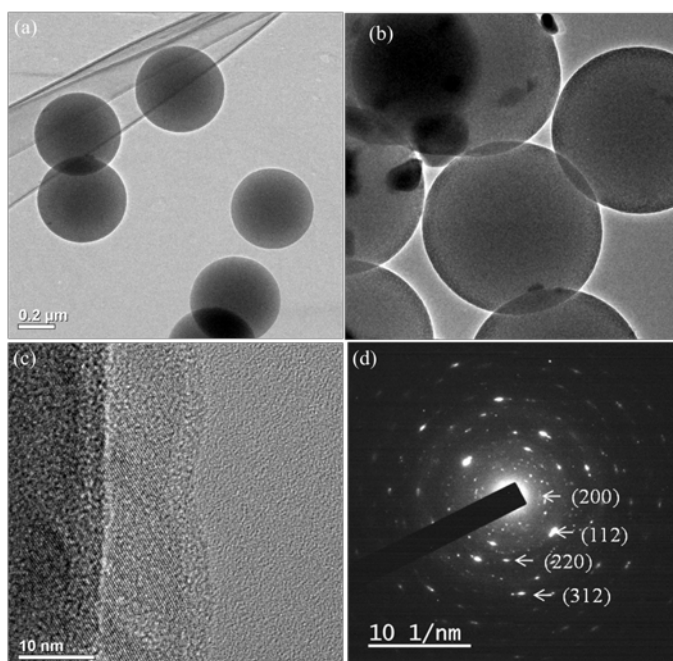


Fig. 4.4 HRTEM images of (a) SiO_2 core, (b) Core shell $\text{YVO}_4:\text{Eu}^{3+}@\text{SiO}_2$ phosphors, (c) interface of the core/shell and (d) SAED of $\text{YVO}_4:\text{Eu}^{3+}@\text{SiO}_2$ phosphors.

Fig. 4.4 shows the HRTEM observation of the SiO_2 core particles, $\text{SiO}_2@Y_{0.96}\text{Eu}_{0.04}\text{VO}_4$ core shell phosphors, crystallized $Y_{0.96}\text{Eu}_{0.04}\text{VO}_4$ and selected area diffraction (SAED) pattern of the core shell phosphor. Fig. 4.4 (a) shows that the formed SiO_2 core particles have spherical shape with an average size of about 400 nm, and it should be noticed that in these particles almost no aggregation can be seen. In part (b) of Fig. 4.4, based on the different electron penetrability for the SiO_2 cores and $Y_{0.96}\text{Eu}_{0.04}\text{VO}_4$ shells, the core-shell structure of $\text{SiO}_2@Y_{0.96}\text{Eu}_{0.04}\text{VO}_4$ particles can be observed clearly. The cores are seen as the black spheres with an average size of 400 nm (similar to the pure SiO_2 particles in Fig. 4.4 (a)) and the shells have gray color with an average thickness of 30-50 nm. In the Fig. 4.4 (c) the interface of core/shell phases can be seen. In addition, the crystalline lines of $Y\text{VO}_4:\text{Eu}^{3+}$ layer indicates the proper crystallinity of this phosphor on the silica cores. This figure is well matched with the XRD spectrum and EDS spectra of the core shell phosphor (which were explained elsewhere) and confirms that well crystallized $Y\text{VO}_4:\text{Eu}^{3+}$ layer has been formed on the amorphous silica cores, significantly. The selected area electron diffraction pattern of the core/shell particles is labeled (see Fig. 4.4 (d)) and demonstrates the existence of crystalline phase ($Y\text{VO}_4$) on the surface of SiO_2 core particles.

4.3.4. FT- IR

The FT-IR spectra of the as-formed fresh SiO_2 , 900 °C annealed pure $\text{YVO}_4:\text{Eu}^{3+}$ powder and $\text{YVO}_4:\text{Eu}^{3+}@\text{SiO}_2$ core-shell phosphor samples are shown in parts a–c of Figure, respectively.

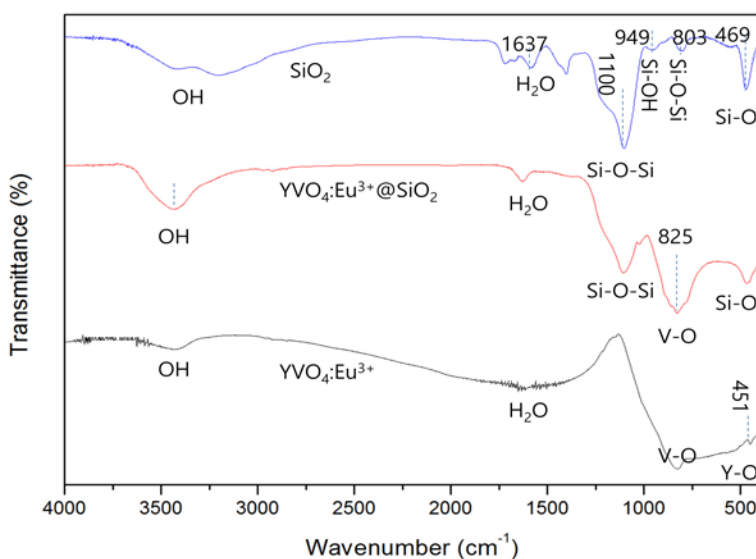


Fig. 4.5 FT-IR spectra of SiO_2 core, Core shell $\text{YVO}_4:\text{Eu}^{3+}@\text{SiO}_2$ phosphors and pure $\text{YVO}_4:\text{Eu}^{3+}$ phosphors.

In the spectrum related to the as-formed fresh SiO_2 particles, the absorption bands due to OH (3435 cm^{-1}), H_2O (1634 cm^{-1}), Si–O–Si (ν_{as} , 1100 cm^{-1} ; ν_{s} , 807 cm^{-1}), Si–OH(ν_{s} , 950 cm^{-1}), and Si–O (δ , 471 cm^{-1}) bonds (where ν_{as} =

asymmetric stretching, ν_s = symmetric stretching, δ = bending) are observed [101]. The mentioned peak absorptions indicate that the fresh SiO_2 particles contain a remarkable value of hydroxide (OH) groups and water (H_2O) on their surfaces [69]. The Si–OH groups on the surface play a very important role for bonding the metal ions (Y^{3+} , Eu^{3+}) from the coating sol and forming the $\text{YVO}_4\text{:Eu}^{3+}$ layers on the amorphous silica surfaces in the following annealing process, as it was shown in Fig.1. In the middle FT-IR spectrum for pure $\text{YVO}_4\text{:Eu}^{3+}$ powders, a strong absorption peak at 832 cm^{-1} and a weak one at 453 cm^{-1} have appeared, which are attributed to the absorption of V–O (from VO_4^{3-} group) and Y(Eu)–O bonds, respectively [102]. These peaks indicate that crystalline phase (YVO_4) has formed after annealing at $900\text{ }^\circ\text{C}$, agreeing well with the results of XRD. For the $\text{YVO}_4\text{:Eu}^{3+}\text{@SiO}_2$ core–shell sample, the characteristic absorption peaks of the V–O bond (832 cm^{-1}) for $\text{YVO}_4\text{:Eu}^{3+}$ and the Si–O–Si bond (1114 cm^{-1}) for amorphous SiO_2 can be observed easily, and the weak signal from the Y–O bond may be affected and covered by the bending vibration of Si–O bond at 471 cm^{-1} . The signal of OH groups from the as-formed silica particles have disappeared completely in the $900\text{ }^\circ\text{C}$ annealed $\text{YVO}_4\text{:Eu}^{3+}\text{@SiO}_2$ core–shell particles. These results are well matched with XRD spectra, EDS analysis and HRTEM image and further demonstrate the formation of crystallized $\text{YVO}_4\text{:Eu}^{3+}$ coatings on the silica surfaces via the sol–gel deposition and annealing process. [67]

4.3.5. PL

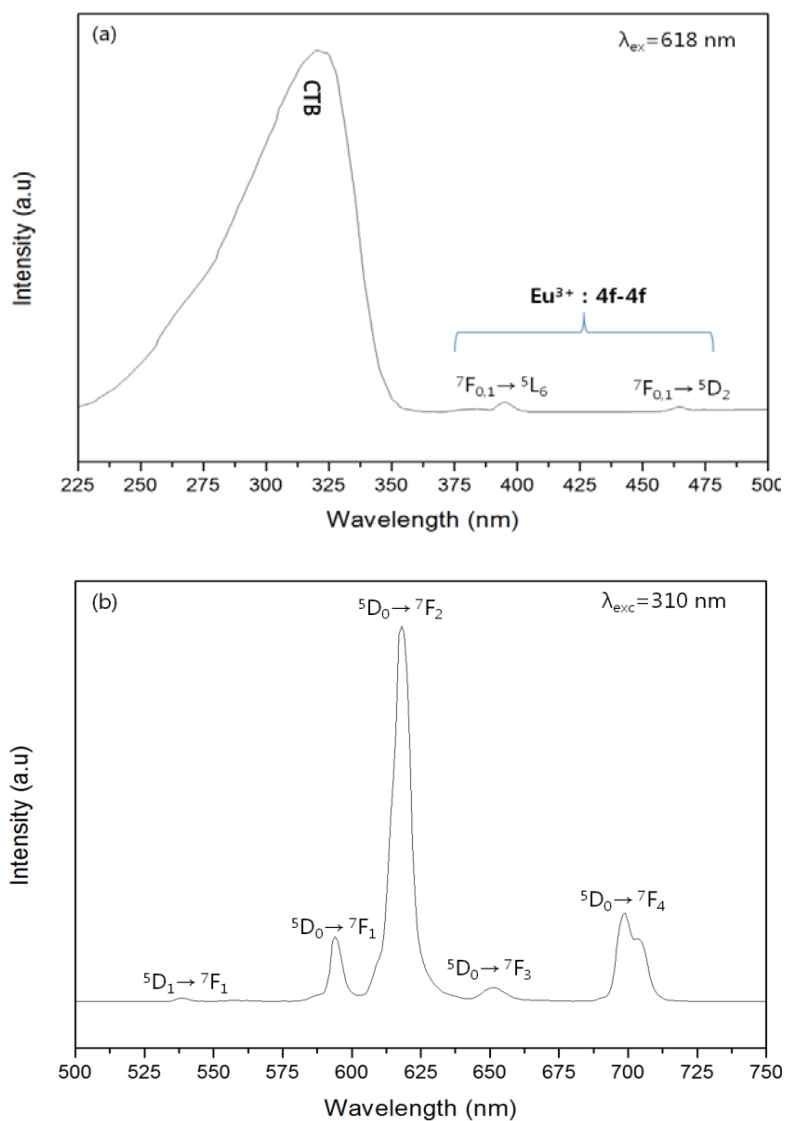


Fig. 4.6 PL (a) excitation and (b) emission spectra of Core shell $\text{YVO}_4:\text{Eu}^{3+}@\text{SiO}_2$ phosphors after 5 times of coating.

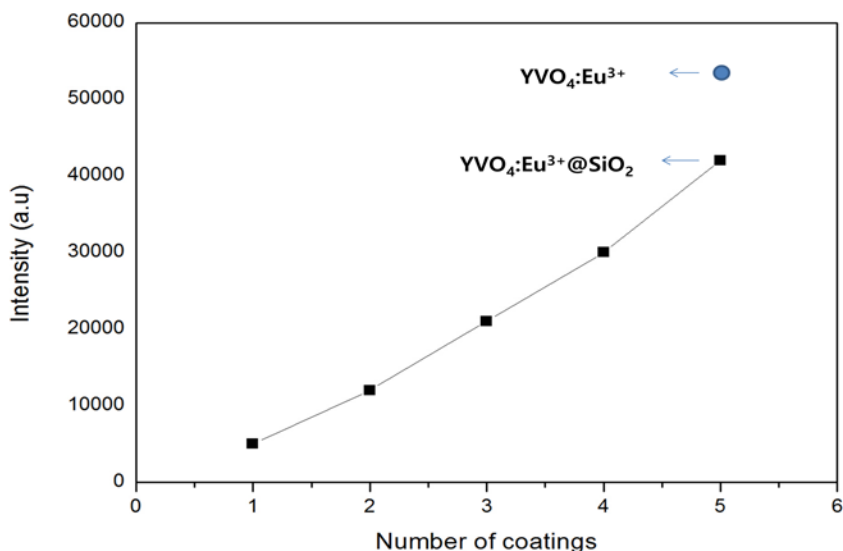


Fig. 4.7 The photoluminescence emission intensity of $\text{YVO}_4:\text{Eu}^{3+}@\text{SiO}_2$ phosphor as a function of the number of coatings (N).

The $\text{SiO}_2@\text{Y}_{0.96}\text{Eu}_{0.04}\text{VO}_4$ core-shell particles exhibit a strong red emission under UV irradiation. Fig. 4.6 shows the excitation (a) and emission (b) spectra of this core-shell particles after calcination at 900 °C for 2 h. The excitation spectrum (Fig. 4.6 (a)) consists of a very broad, intense band ranging from 200 to 350 nm with a maximum 320 nm and some relatively weaker lines in the longer wavelength region. The former can be attributed to the YVO_4 host excitation band, together with the $\text{Eu}^{3+} - \text{O}^{2-}$ charge transfer band, and the later is belong to the f-f transitions within Eu^{3+} ($4f^6$) electron configuration (main peaks at the 393 and 464 nm corresponding to the electron transitions from

the 7F_0 ground state to 5L_6 and 5D_2). The presence of the strong YVO_4 host band in the excitation spectrum of Eu^{3+} indicates that there exists an energy transfer from YVO_4 host to the doped Eu^{3+} . Also, the emission spectrum of this phosphor material consists of some sharp peaks in the region 350–750 nm, as detailed in Fig. 4.6 (b). The lines belong to transitions between the energy levels of the $4f^6$ configuration of Eu^{3+} ion and it is clear that the spectrum is dominated by the main lines at 618 nm due to the ${}^5D_0 - {}^7F_2$ transition and 593 nm due to the ${}^5D_0 - {}^7F_1$ transition. The peaks from the electric-dipole transition (${}^5D_0 - {}^7F_2$) is relatively stronger than that from magnetic-dipole transition (${}^5D_0 - {}^7F_1$). It is well known that when the Eu^{3+} ion is located at crystallographic site without inversion symmetry, its hypersensitive transition ${}^5D_0 - {}^7F_2$ red emission will dominate in the emission spectrum; otherwise, if the Eu^{3+} site has an inversion center, its ${}^5D_0 - {}^7F_1$ (orange) emission will dominate. Apparently, in $SiO_2@Y_{0.96}Eu_{0.04}VO_4$ core-shell particle phosphors, the Eu^{3+} will replace the Y^{3+} in view of their similar sizes [$r(Eu^{3+}) = 0.095$ nm, $r(Y^{3+}) = 0.094$ nm]. Since the Eu^{3+} ions are located at sites without inversion symmetry in this core-shell particles, it is expected that the ${}^5D_0 - {}^7F_2$ transition will dominate in the emission spectra. In addition, the emission lines from higher excited states of Eu^{3+} (5D_1) can also be observed in the core-shell particles. This can be ascribed to the fact that the low vibration energy of VO_4^{3-} group is not able to bridge the gaps between the higher energy level 5D_1 and the 5D_0 level of Eu^{3+} completely. Noteworthy, it is obvious that although the thickness of formed phosphor on the

surface of uniform SiO_2 particles is in the range of 30-50 nm, but a perfect spectrum of photoluminescence was obtained by exciting the phosphor under 320 nm. Also, Fig. 4.7 indicates that after few times of $\text{YVO}_4:\text{Eu}^{3+}$ coating on SiO_2 cores the photoluminescence emission is comparable to that of pure $\text{YVO}_4:\text{Eu}^{3+}$ phosphor that is synthesized via sol-gel method. This issue indicates that $\text{YVO}_4:\text{Eu}^{3+}$ phosphor with a well crystallized form has been formed on SiO_2 cores. In addition, the spherical morphology with a smooth surface of the core/shell phosphor can enhance the luminescence properties significantly.

4.3.6. SiO₂ coated YVO₄:Eu³⁺@SiO₂ phosphors

A typical synthesis process was as follows: a mixture of C₂H₅OH (40 ml) and H₂O (8 ml) was prepared in a beaker followed by addition of 4 ml ammonia to be mixed well for 1 h at 60°C. The pH of the solution was fixed in the range of 8-9 by adding proper amounts of citric acid solution. During preparation of the solution, both of temperature and the amounts of pH were under control by a digital and accurate temperature and pH meter. As a typical procedure, 1 g (estimated) of YVO₄: Eu³⁺ phosphor in the YVO₄:Eu³⁺@SiO₂ phosphors powder was dispersed into the above beaker, and they were gently stirred at 60 °C for 1 h. Tetraethylorthosilicate (TEOS) in different volume was added into the above beaker under stirring, and the adding amount was 0.5 wt%, 1 wt%, 2 wt% and 4 wt%, respectively, corresponding to the amount of YVO₄: Eu³⁺ phosphor. After being stirred for 2 h, these phosphor powders were washed 3 times by ethanol, dried in an oven at 100 °C for 12 h and annealed at 900 °C for 3 h. Finally, SiO₂-coated YVO₄: Eu³⁺phosphors with various SiO₂ addition content (0.5 wt%, 1 wt%, 2 wt% and 4 wt %) were obtained. For getting these coated phosphors 18.6, 37.2, 74.4 and 148.8 µl TEOS were added, respectively. As a comparison, the un-coated YVO₄:Eu³⁺@SiO₂ phosphor too experienced the same drying process at 100 °C for 12 h and calcination process at 900 °C for 3 h.

4.3.6.1. XRD Analysis

Fig. 4.8 shows the XRD patterns of sol-gel synthesized $\text{SiO}_2@Y_{0.96}\text{Eu}_{0.04}\text{VO}_4$ core-shell particle phosphors with different amounts of silica coating. The sol-gel synthesized samples show that they are well crystallized and have a tetragonal crystal structure (JCPDS 72-0861). In addition, the XRD patterns are similar without any new phase formation even in the presence of the relatively higher amounts of SiO_2 . Then, it can be found that the XRD pattern of $\text{SiO}_2@Y_{0.96}\text{Eu}_{0.04}\text{VO}_4$ core-shell phosphors does not show any change within coating with silica.

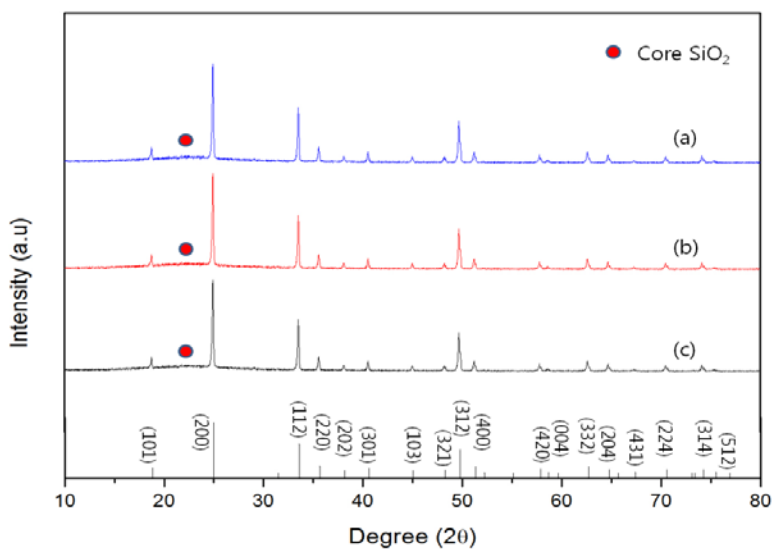


Fig. 4.8 XRD spectra of $\text{SiO}_2@Y_{0.96}\text{Eu}_{0.04}\text{VO}_4$ with different amounts of silica coating: (a) 0 wt%, (b) 1 wt% and (c) 2 wt%.

4.3.6.2. FESEM Observation

Fig. 4.9 shows the FESEM images of $\text{SiO}_2@\text{Y}_{0.96}\text{Eu}_{0.04}\text{VO}_4$ coated with 1 wt% silica at different magnifications. Fig. 4.9 (a) shows that the synthesized phosphor has a spherical morphology in the range of 350-400 nm.

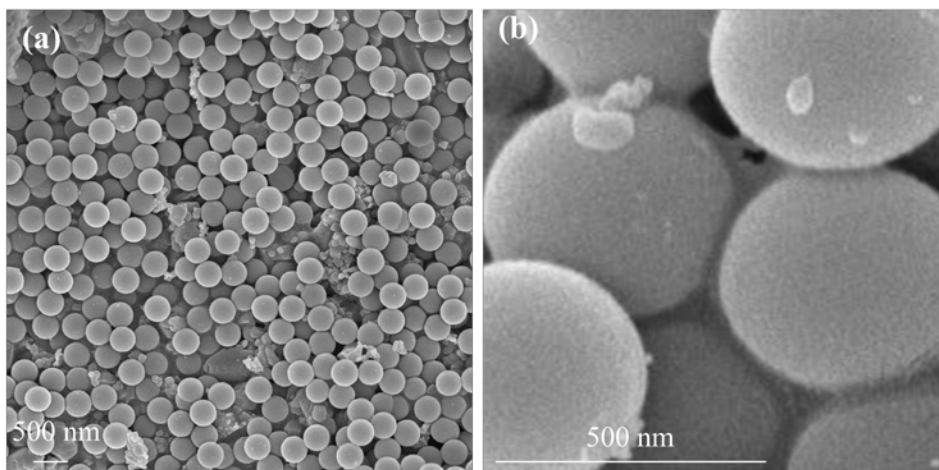


Fig. 4.9 FESEM images of $\text{SiO}_2@\text{Y}_{0.96}\text{Eu}_{0.04}\text{VO}_4$ coated with 1 wt% silica at different magnifications.

Part (b) of Fig. 4.9 and EDS analysis confirm the formation of very small particles of silica on the surface of $\text{SiO}_2@\text{Y}_{0.96}\text{Eu}_{0.04}\text{VO}_4$ phosphors. It can be seen that SiO_2 coated $\text{SiO}_2@\text{Y}_{0.96}\text{Eu}_{0.04}\text{VO}_4$ phosphors still keep the spherical morphology of the silica particles, and still no agglomeration can be found in the FESEM image. This observation is well matched with XRD spectrum of the core shell phosphor and shows that $\text{YVO}_4:\text{Eu}^{3+}$ layer is well formed on the amorphous silica cores but since the amounts of coated silica on the surface is small, the related peak in the XRD spectra cannot be seen. However, it should be

mentioned that the FESEM micrographs can only provide the preliminary information on the morphology of phosphor particles in large scale and the core-shell structure of $\text{SiO}_2@\text{Y}_{0.96}\text{Eu}_{0.04}\text{VO}_4$ particles and the silica coated ones cannot be well studied and resolved from the FESEM micrographs based on the limitations of magnification.

4.3.6.3. TEM Observation

To study the core-shell-shell structure of SiO_2 coated $\text{SiO}_2@\text{Y}_{0.96}\text{Eu}_{0.04}\text{VO}_4$ phosphors more accurately, the HRTEM analysis was employed.

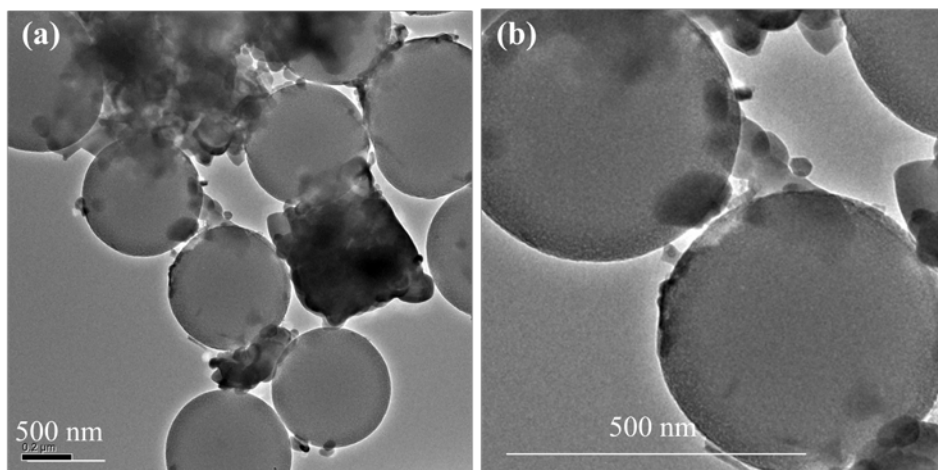


Fig. 4.10 HRTEM images of $\text{SiO}_2@\text{Y}_{0.96}\text{Eu}_{0.04}\text{VO}_4$ coated with 1 wt% silica at different magnifications.

Fig. 4.10 shows the HRTEM observation of the SiO_2 coated $\text{SiO}_2@\text{Y}_{0.96}\text{Eu}_{0.04}\text{VO}_4$ phosphors. In part (b) of Fig. 4.10 the core/shell structure

can be seen, clearly. In addition, the formation of individual small silica particles on the surface of the core/shell phosphors was confirmed by the EDS analysis.

4.3.6.4. PL Analysis

Fig. 4.10 shows that coating of $\text{YVO}_4:\text{Eu}^{3+}@\text{SiO}_2$ core shell phosphors with silica decrease the emission intensity. It was shown elsewhere that in the $\text{YVO}_4:\text{Eu}^{3+}@\text{SiO}_2$ core shell structure, the thickness of formed $\text{YVO}_4:\text{Eu}^{3+}$ on the surface of silica is low and it is in the range of 15-35 nm. In addition, referring to relatively small size of core shell phosphors, it is possible that some parts of silica surface remain bare without any phosphor coverage.

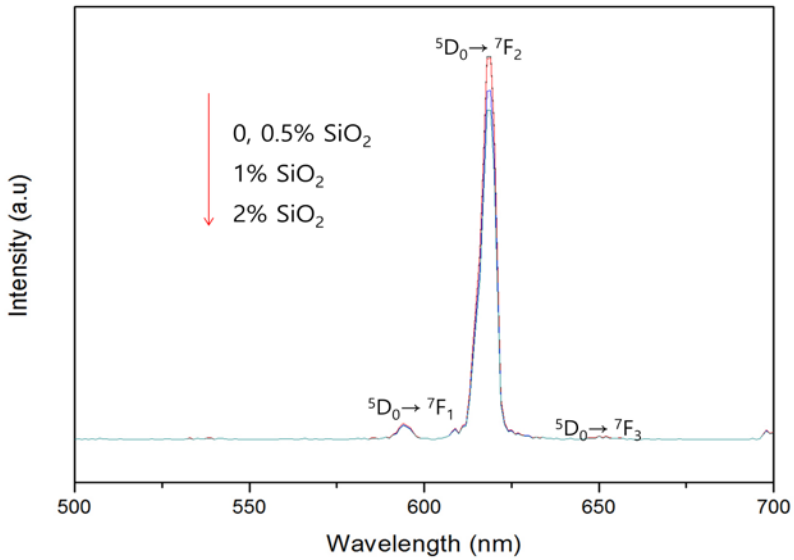


Fig. 4.11 Photoluminescence emission properties of SiO_2 coated $\text{YVO}_4:\text{Eu}^{3+}@\text{SiO}_2$ phosphors with different amounts of silica.

So, it seems that coating of silica on $\text{YVO}_4:\text{Eu}^{3+}@\text{SiO}_2$ core shell particles cannot be done properly. Even the silica coating of core shell particles can

decrease the roundness of these phosphors and it is already known that using spherical phosphors results in high packing density and low scattering of light [102].

4.3.6.5. Chemical Stability

Recent studies show that $\text{YVO}_4:\text{Eu}^{3+}$ has significant promise in plasma display panels (PDP) [81]. Recently, LnVO_4 ($\text{Ln} = \text{Y}, \text{La}, \text{Gd}$ and Lu) materials have attracted much attention in PDP applications due to their high thermal and chemical stability and high luminescence efficiency under VUV excitation [82]. Also, for the phosphors used in PDP industries chemical stability is one of the critical properties [83]. As an specific procedure, 0.25 g uncoated and 0.25 g of 1 wt% SiO_2 -coated $\text{YVO}_4:\text{Eu}^{3+}$ @ SiO_2 phosphors into two series of beakers filled with of HNO_3 (1 ml of 95% acid) and HCl (8.5 of 35% acid) and then 15 ml of de-ionized water was added to all of beakers at the same time. Accordingly, after the immersion in the mixture of acid for 15 min, it was followed by separation through centrifuge at the speed of 3000 rpm for 5 min. The acid was analyzed by ICP to measure the amounts of dissolved elements and the remained powders were washed by de ionized water 3 times. Table 4.1 shows the ICP data of both coated and uncoated phosphors and it is obvious that coating of phosphors with silica somehow prohibits the dissolution of $\text{YVO}_4:\text{Eu}^{3+}$ phosphor. In other words, the concentration of Y, V and Eu in acid is higher in the case of bare phosphors than those of coated one. For example the amounts of Yttrium

elements of bare $\text{YVO}_4:\text{Eu}^{3+}$ phosphor is 102.11 ppm in the acid solution while it reduced to 82.35 and 63.17 for $\text{YVO}_4:\text{Eu}^{3+}\text{-2\%SiO}_2$ and $\text{YVO}_4:\text{Eu}^{3+}\text{-4\%SiO}_2$ phosphors, respectively. This data shows the protection of phosphor particles in aggressive mediums very well.

Table 4.1 the amounts of elements (ppm) of bare and coated $\text{YVO}_4:4\%\text{Eu}^{3+}$ phosphors in the acid mixture solution.

Composition	Y	V	Eu	Si
$\text{YVO}_4:\text{Eu}^{3+}\text{@SiO}_2$	82.37	79.32	6.91	3.65
SiO_2 coated $\text{YVO}_4:\text{Eu}^{3+}\text{@SiO}_2$	69.95	68.24	5.88	7.12

Also, the morphology of collected phosphor powders was studied by the FESEM right after drying at 100 °C (not shown here). It was found that bare phosphors have been solved partially in acid media but conversely, we could not see a remarkable difference between the size of coated phosphor particles before and after soaking in the acid mixture.

4.3.6.6. Thermal quenching

As it was explained elsewhere, the temperature of the substrate of LED lamps usually increases to about 150 °C and even higher for street lamps, because heat

is produced continuously during LED operation. The thermal stability of LED depends strongly on the used phosphors [85]. It is known that the luminescent ion can reach the ground state via thermal quenching. The thermal quenching of $\text{YVO}_4:\text{Eu}^{3+}$ activated phosphors at higher temperatures is due to the excited electrons easily jumping into the CTS band after absorbing thermal energy, at which the probability of non-radiative transition may increase. Thus, the emission intensity of Eu^{3+} activated phosphors decreases with increasing temperature. The activation energy of $\text{YVO}_4:\text{Eu}^{3+}$ is smaller than that of silica coated one, indicating that the former is more sensitive to the thermal effect. It is expected that the activation energy of the bare $\text{YVO}_4:\text{Eu}^{3+}@\text{SiO}_2$ phosphors is smaller than that of the silica coated one, indicating that the coating of SiO_2 on the surface of $\text{YVO}_4:\text{Eu}^{3+}@\text{SiO}_2$ phosphors increase the thermal resistant and suppress the thermal quenching [86]. Fig. 4.12 clearly shows that coating the phosphor with SiO_2 decrease the thermal quenching effect. In other words, silica coating results in higher resistance to the thermal quenching due to the formation of a protective layer on the surface of phosphor. In fact for the bare $\text{YVO}_4:\text{Eu}^{3+}$ phosphors, the intensity of $^5\text{D}_0\text{-}^7\text{F}_2$ peak reduced about 10% when the temperature increased from 25 to 175 °C.

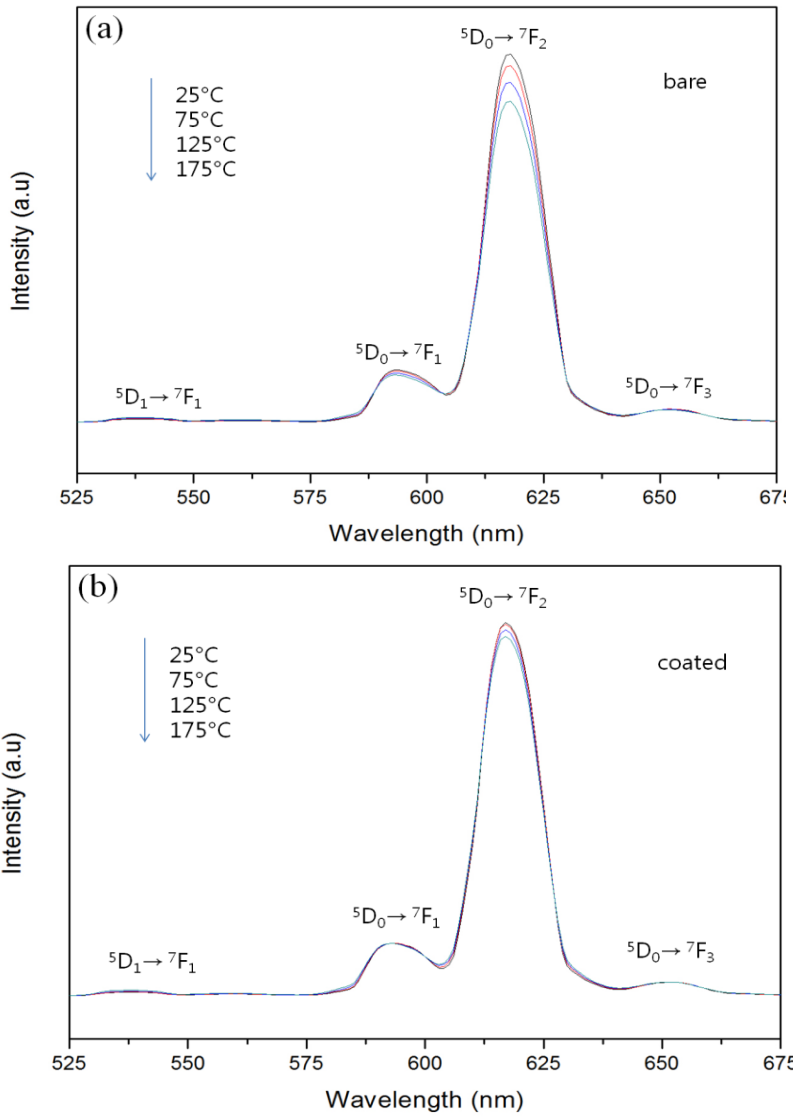


Fig. 4.12 Temperature dependent Photoluminescence emission spectra of $\text{YVO}_4:\text{Eu}^{3+}$ phosphors (a) without 1 wt% SiO_2 , (b) with SiO_2 and (c) the combination of parts (a) and (b).

In summarize, the results indicate that the value of T50 for these phosphors is above 175°C, indicating that these phosphors have good thermal stability; the thermal stability of coated phosphor is superior to that of bare phosphor.

4.4. Summary and conclusion

In this research, $\text{YVO}_4:\text{Eu}^{3+}@\text{SiO}_2$ core/shell phosphors were successfully synthesized with a very uniform size of 350-400 nm. After 5 times coating of $\text{YVO}_4:\text{Eu}^{3+}$ on SiO_2 cores, the luminescence properties is comparable to that of pure $\text{YVO}_4:\text{Eu}^{3+}$ phosphors. Also, coating of $\text{YVO}_4:\text{Eu}^{3+}@\text{SiO}_2$ Core/shell phosphor with a layer of SiO_2 was done successfully through sol-gel method.

Although the silica coating of $\text{YVO}_4:\text{Eu}^{3+}@\text{SiO}_2$ phosphor, decrease the luminescence slightly, but the thermal quenching resistant was improved, significantly.

V. Overall Conclusion

Micron sized $\text{YVO}_4:\text{Eu}^{3+}$ phosphor was synthesized via the simple solid state method and it was found that un-doped YVO_4 material synthesized in the air atmosphere shows a luminescence property under the excitation wavelength of 310 nm, due to the formation of many defects. In addition, although $\text{YVO}_4:\text{Eu}^{3+}$ phosphor showed a brilliant red emission with monitoring by the wavelength of 310 nm, but the ESR studies showed that the surface of this phosphor contains a lot of defects. Then, to decrease the surface defects, $\text{YVO}_4:\text{Eu}^{3+}$ phosphor was coated by silica through the sol-gel method. It was found that silica coating yields an increase in luminescence intensity of the phosphors due to the reduction of defects and also the reduction of reflection of excitation light. The maximum amount of emission intensity was obtained with 1 wt% silica coating and hence the quantum efficiency was enhanced by 11%. At more amounts of coating, the thickness of coating layer is relatively higher and it results in absorbance of light by the coating layer and then much loss of brightness and photoluminescence emission. Furthermore, the coating of $\text{YVO}_4:\text{Eu}^{3+}$ phosphors by silica enhanced the chemical stability and resistant to the thermal quenching at higher temperatures. Furthermore, $\text{YVO}_4:\text{Eu}^{3+}@\text{SiO}_2$ core/shell phosphors were successfully synthesized with a very uniform size of 350-400 nm. After 5 times coating of $\text{YVO}_4:\text{Eu}^{3+}$ on SiO_2 cores, the luminescence properties is comparable to that of pure $\text{YVO}_4:\text{Eu}^{3+}$ phosphors. Also, coating of $\text{YVO}_4:\text{Eu}^{3+}@\text{SiO}_2$ Core/shell phosphor with a layer of SiO_2 was done

successfully through sol-gel method. Although the silica coating of $\text{YVO}_4:\text{Eu}^{3+}@\text{SiO}_2$ phosphor, decrease the luminescence slightly, but the thermal quenching resistant was improved, significantly.

Appendix

Table 1 Physical properties of SiO₂

Molecular formula	SiO ₂
Molar mass	60.08 g/mol
Appearance	Transparent crystals
Density	2.648 g·cm ⁻³
Melting point	1,600- 1,725 °C
Thermal conductivity	0.01 W/cm K (bulk)
Refractive index	1.46 [thermal oxide]
Dielectric constant	3.9 [thermal oxide]; CVD oxides vary widely depending on H

References

1. X. Rong-Jun, H. Naoto, Silicon-based oxynitride and nitride phosphors for white LEDs—A review. *Sci. Technol. Adv. Mater.* 8 (2007), 588–600.
2. G. Hirata, Luminescence study in Eu-doped aluminum oxide phosphors, *Optical Materials*. 27(2005), 1311–1315.
3. R. Dey, V. Kumar Rai, Yb^{3+} sensitized Er^{3+} doped La_2O_3 phosphor in temperature sensors and display devices, *The Royal Society of Chemistry 2014 Dalton Trans.* 43(2014), 111–118.
4. J. Sokolnicki. Rare earths (Ce, Eu, Tb) doped $\text{Y}_2\text{Si}_2\text{O}_7$ phosphors for white LED, *Journal of Luminescence*. 134(2013), 600–606.
5. K.V.R. Murthy, A.S. Sai Prasad, M. Ramaligeshwar Rao. Luminescence Characteristics of Eu and Tb Doped YGdBO_3 Phosphor, *Physics Procedia*. 29(2012), 70–75.
6. S. Uysal Satilmis, A. Ege, M. Ayvacikli, A. Khatab, E. Ekdal, E.J. Popovici, M. Henini, N. Can Luminescence characterization of cerium doped yttrium gadolinium aluminate phosphors, *Optical Materials*. 34(2012), 1921–1925.
7. G.A. Kumar, M. Pokhrel, D.K. Sardar. Absolute quantum yield measurements in Yb/Ho doped $\text{M}_2\text{O}_2\text{S}$ ($\text{M}=\text{Y}, \text{Gd}, \text{La}$) up-conversion phosphor, *Materials Letters*. 98(2013), 63–66.
8. A. Pandey, V. Kumar Rai. Colour emission tunability in $\text{Ho}^{3+}\text{--Tm}^{3+}\text{--Yb}^{3+}$ co-doped Y_2O_3 upconverted phosphor, *Appl. Phys. B* 109 (2012), 611–616.
9. S. Ekambaram, K.C. Patil, M. Maaza. Synthesis of lamp phosphors: facile combustion approach, *J. Alloys and Compounds*. 393(2005), 81–92.

10. L. Hui-Li, H. Naoto, X. Rong-Jun, S. Takayuki, M. Mamoru. Fine yellow α -SiAlON:Eu phosphors for white LEDs prepared by the gas-reduction–nitridation method, *Sci. Techno. Adv. Mater.* 8 (2007), 601-606.
11. R. Kane, H. Sell. *Revolution in lamps: a chronicle of 50 years of progress* (2nd edition), The Fairmont Press, Inc. 2001 ISBN 0-88173-378-4.
12. R. Balakrishnaiah. Enhanced luminescence properties of $\text{YBO}_3\text{:Eu}^{3+}$ phosphors by Li-doping, *Materials Research Bulletin* 46(2011) 621–626.
13. X. Wu. et al. Morphological Control and Luminescent Properties of $\text{YVO}_4\text{:Eu}$ Nanocrystals, *J Phys Chem B* 110 (2006), 15791-15796.
14. L. Tian, S. Mho. Enhanced Photoluminescence of $\text{YVO}_4\text{:Eu}^{3+}$ by codoping the Sr^{2+} , Ba^{2+} or Pb^{2+} ion. *J Lumin* 122-123(2007), 99-103.
15. B. Yan, $\text{YVO}_4\text{:RE}^{3+}$ (RE= Eu, Sm, Dy, Er) nanophosphors: facile hydrothermal synthesis, microstructure and photoluminescence, *J Mater Res* 24(2009), 3050-3056.
16. J.W. Stouwdam, M. Raudsepp, F. van Veggel. Colloidal nano-particles of LaVO_4 : Energy transfer to visible and near-infrared emitting lanthanide ions *Langmuir* 21(2005), 7003-7008.
17. L. Yang, G. Li, M. Zhao, E. Yang and L. Li. Lattice defect quenching effects on luminescence properties of Eu^{3+} -doped YVO_4 nanoparticles, *J Nanopart Res* 15(2013), 1-12.
18. B. Kumar Grandhe. Enhanced red emission from $\text{YVO}_4\text{:Eu}^{3+}$ nano phosphors prepared by simple Co-Precipitation Method, *Electronic Materials Letters* June 7(2011), 161-165.
19. L. Li, M. Zhao, W. Tong, X. Guan, G. Li and L. Yang. Preparation of cereal-like $\text{YVO}_4\text{:Ln}^{3+}$ (Ln = Sm, Eu, Tb, Dy) for high quantum efficiency photoluminescence, *Nanotechnology* 21(2010), 1-8.

20. D. Chen, Y. Yu, P. Huang, H. Lin, Z. Shan, L. Zeng, A. Yang, and Y. Wang, Color-tunable luminescence for $\text{Bi}^{3+}/\text{Ln}^{3+}:\text{YVO}_4$ ($\text{Ln} = \text{Eu}, \text{Sm}, \text{Dy}, \text{Ho}$) nanophosphors excitable by near-ultraviolet light. *Phys. Chem. Chem. Phys.* 12 (2010), 7775-7778.
21. L. Chen, K. J. Chen, C. C. Lin, C. I. Chu, S. F. Hu, M. H. Lee, and R. S. Liu. Combinatorial approach to the development of a single mass $\text{YVO}_4:\text{Bi}^{3+}, \text{Eu}^{3+}$ phosphor with red and green dual colors for high color rendering white light-emitting diodes, *J. Comb. Chem.* 12(2010), 587-594.
22. N. S. Singh, R. S. Ningthoujam, M. N. Luwang, S. D. Singh, and R. K. Vatsa. Luminescence, lifetime and quantum yield studies of $\text{YVO}_4:\text{Ln}^{3+}$ ($\text{Ln}^{3+} = \text{Dy}^{3+}, \text{Eu}^{3+}$) nanoparticles: Concentration and annealing effects, *Chem. Phys. Lett.* 480(2009), 237-242.
23. A.H. Krumpel, P. Boutinaud, E. van der Kolk, and P. Dorenbos, Charge transfer transitions in the transition metal oxides $\text{ABO}_4:\text{Ln}^{3+}$ and $\text{APO}_4:\text{Ln}^{3+}$ ($\text{A}=\text{La}, \text{Gd}, \text{Y}, \text{Lu}, \text{Sc}$; $\text{B}=\text{V}, \text{Nb}, \text{Ta}$; $\text{Ln}=\text{lanthanide}$), *J. Lumin.* 130 (2010), 1357-1365.
24. G. Pan, H. Song, X. Bai, Z. Liu, H. Yu, W. Di, S. Li, L. Fan, X. Guang Ren, and Shaozhe Lu. Novel Energy-Transfer Route and Enhanced Luminescent Properties in $\text{YVO}_4:\text{Eu}^{3+}/\text{YBO}_3:\text{Eu}^{3+}$ Composite, *Chem. Mater.* 18 (2006), 4526–4532.
25. Y.H. Zhou, J. Lin. Morphology control and luminescence properties of $\text{YVO}_4:\text{Eu}$ phosphors prepared by spray pyrolysis, *Optical Materials.* 27(2005), 1426–1432.
26. M. Yu, J. Lin, J. Fu, H. J. Zhang and Y. C. Han. Sol–gel synthesis and photoluminescent properties of $\text{LaPO}_4:\text{A}$ ($\text{A} = \text{Eu}^{3+}, \text{Ce}^{3+}, \text{Tb}^{3+}$) nanocrystalline thin films, *J. Mater. Chem.* 13(2003), 1413-1419.
27. G. Blasse, A. Bril. On the Eu^{3+} Fluorescence in Mixed Metal Oxides. II the $^5\text{D}_0\text{-}^7\text{F}_0$ Emission, *Philips Res. Repts.* 21(1966), 368-378.

28. F. Zhang, S. Chan, J.E. Spanier, E. Apak, Q. Jin, R. D. Robinson and I. P. Herman. Cerium oxide nanoparticles: Size-selective formation and structure analysis, *Appl. Phys. Lett.* 80 (2002), 127-129.
29. G. S. Li, B. Goates, J. Woodfield, B. Li. Evidence of linear lattice expansion and covalency enhancement in rutile TiO₂ nanocrystals. *Appl. Phys. Lett.* 85(2004), 2059–2061.
30. G. Hodes. When Small Is Different: Some Recent Advances in Concepts and Applications of Nanoscale Phenomena, 19(2007), 639–655.
31. Y.K. Voron'ko, A.A. Sobol, V.E. Shukshin, A.I. Zagumennyĭ, Y.D. Zavartsev, S.A. Kutovoĭ. Raman Spectroscopic Study of Structural Disorder in YVO₄, GdVO₄, and CaWO₄ Crystals. *Phys. Solid State*, 51(2009), 1886-1893.
32. K. N. Yu, Y. Xiong, Y. Liu, and C. Xiong. Microstructural change of nano-SnO₂ grain assemblages with the annealing temperature, *Phys. Rev. B* 55(1997), 2666–2671.
33. L. Yang et.al. Control Over the Crystallinity and Defect Chemistry of YVO₄ Nanocrystals for Optimum Photocatalytic Property, *Euro J Inorganic Chemistry*, 2011(2011), 2211–2220.
34. H. Wu, H. Xu, Q. Su, T. Chen and M. Wu. Size- and shape-tailored hydrothermal synthesis of YVO₄ crystals in ultra-wide pH range conditions, *J. Mater. Chem.*, 13(2003), 1223-1228.
35. B. C. Chakoumakos, M. M. Abraham, and L. A. Boatner, “Crystal structure refinements of zircon-type MVO₄ (M = Sc, Y, Ce, Pr, Nd, Tb, Ho, Er, Tm, Yb, Lu),” *J. Solid State Chem.* 109(1994), 197–202.
36. X. Meng, L. Zhu, H. Zhang, C. Wang, Y. T. Chow, and M. Lu. Growth, morphology and laser properties of Nd:YVO₄ crystal, *J. Cryst. Growth* 200(1999), 199–203.
37. L. Millet, J.P. Borel. Spin susceptibility of small Mg particles measured

- by CESR, Surface Science. 106(1981), 403–407.
38. R. Kubo. Electronic Properties of Metallic Fine Particles. I. J. Phys. Soc. Jpn. 17 (1962), 975-986.
 39. T. Hirai, T. Hirano, I. Komasaawa. Preparation of Gd_2O_3 : Eu^{3+} and $\text{Gd}_2\text{O}_2\text{S}$: Eu^{3+} Phosphor Fine Particles Using an Emulsion Liquid Membrane System, J. Colloid Interface Sci. 253 (2002), 62–69.
 40. Q. Li, L. Gao, D.S. Yan. Effects of the Coating Process on Nanoscale Y_2O_3 : Eu^{3+} Powders, Chem. Mater. 11 (1999), 533–535.
 41. C. Guo, B. Chu, M. Wu, Q. Su. Oxide coating for alkaline earth sulfide based phosphor, Journal of Luminescence. 105 (2003), 121–126.
 42. M. Niraj, R. Singh Ningthoujam, S. Krishna Srivastava and R. Kumar Vatsa. Preparation of white light emitting YVO_4 : Ln^{3+} and silica-coated YVO_4 : Ln^{3+} ($\text{Ln} = \text{Eu}, \text{Dy}, \text{Tm}$) nanoparticles by CTAB/n-butanol/hexane/water microemulsion route: Energy transfer and site symmetry studies, J. Mater. Chem. 21(2011), 5326–5337.
 43. H. Liu, Z. Xia, J. Zhuang, Z. Zhang, L. Liao. Surface treatment investigation and luminescence properties of SiO_2 -coated $\text{Ca}_2\text{BO}_3\text{Cl}$: 0.02Eu^{+2} phosphors via sol–gel process, Journal of Physics and Chemistry of Solids. 73 (2012), 104–108.
 44. F. Li, Y. Yang, Y. Song, W. Wang, W. Yang, and B. Yang. Photoluminescence Spectroscopic Study of $\text{BaMgAl}_{10}\text{O}_{17}$:Eu Phosphor Coated with CaF_2 via a Sol-Gel Process, Journal of Spectroscopy. 2013(2013), 1-5.
 45. H. Seok Lee, J. Whan Yoo. Yellow phosphors coated with TiO_2 for the enhancement of photoluminescence and thermal stability, Applied Surface Science. 257 (2011), 8355–8359.
 46. S. Oh, H. Lee, K. Kim, and J. Kang. Protective Metal Oxide Coatings

- on Zinc-sulfide-based Phosphors and their Cathodoluminescence Properties, *Bull. Korean Chem. Soc.* 31(2010), 3723-3729.
47. T.A. Dang and C.N. Chau. Electron Spectroscopy for Chemical Analysis of Cool White Phosphors Coated with SiO₂ Thin Film, *J. Electrochem. Soc.* 143(1996), 302-305.
 48. T. Ogi, Y. Kaihatsu, F. Iskandar, W. N. Wang, and K. Okuyama, Facile Synthesis of New Full-Color-Emitting BCNO Phosphors with High Quantum Efficiency, *Adv. Mater.* 20(2008), 3235-3238.
 49. W. N. Wang, T. Ogi, Y. Kaihatsu, F. Iskandar, and K. Okuyama, Novel rare-earth-free tunable-color-emitting, BCNO phosphors, *J. Mater. Chem.* 21(2011), 5183-5189.
 50. T. Ogi, A. Bayu Dani, K. Okino, F. Iskandar, W. ang, E. Tanabe, K. Okuyama. Towards Better Phosphor Design: Effect of SiO₂ Nanoparticles on Photoluminescence Enhancement of YAG:Ce, *ECS J. Solid State and Tech.* 2(2013), 91-95.
 51. M. Ikrajuddin, F. Iskandar, K. Okuyama, F. Shi. Stable Photoluminescence of Zinc Oxide Quantum Dots in Silica Nanoparticles Matrix Prepared by the Combined Sol-Gel and Spray Drying Method, *J. Appl. Phys.* 89(2001), 6431-6434.
 52. F. Iskandar, H. Chang, K. Okuyama. Preparation of microencapsulated powders by an aerosol spray method and their optical properties, *Adv. Powder Technol.* 14(2003), 349-367.
 53. Y.C. Kang, H.S. Roh, S.B. Park, Morphology of oxide phosphor particles prepared by colloidal seed-assisted spray pyrolysis, *J. Electrochem. Soc.* 147 (2000), 1601–1603.
 54. Q.X. Liu, Z.H. Xu, J.A. Finch, A Novel Two-Step Silica-Coating Process for Engineering Magnetic Nanocomposites, *Chem. Mater.* 10

- (1998), 3936–3940.
55. Q. Fu, C.G. Lu, J. Liu, Selective Coating of Single Wall Carbon Nanotubes with Thin SiO₂ Layer, *Nano Lett.* 2 (2002) 329–332.
 56. J. Jean. Y₂O₂S:Eu red phosphor powders coated with silica, *J Am Ceram Soc.* 83(2000), 1928-1934.
 57. W. Wang, W. Widiyastuti, I. Wuled Lenggoro, T. Kim and K. Okuyama. Photoluminescence Optimization of Luminescent Nanocomposites Fabricated by Spray Pyrolysis of a Colloid-Solution Precursor, *J. Electrochem. Soc.* 154(2007), 121-128.
 58. G. Liu. silica coated Y₂O₃:Eu nanoparticles and their luminescence properties, *J Lumin*, 126(2007), 702-706.
 59. S. Do. uniform and continuous SiO₂ coating on ZnS phosphor, *Mat. Chem. Phys.* 103(2007), 89-94.
 60. G. Liu, G. Hong, D. Sun. Coating Gd₂O₃:Eu phosphors with silica by solid-state reaction at room temperature, *Powder Technology.* 145(2004), 149–153.
 61. W. Park et al. Thin sio₂ coating on zns phosphors for improved low voltage cathodoluminescence properties, *J. Mater. Res.* 15(2000), 2288-2291.
 62. J.Q. Zhuang, Z.G. Xia, H.K. Liu, Z.P. Zhang, L.B. Liao. The improvement of moisture resistance and thermal stability of Ca₃SiO₄Cl₂:Eu²⁺ phosphor coated with SiO₂, *Appl. Surf. Sci.* 257 (2011), 4350–4353.
 63. Hyoungh-Seok Do, Eun-Jin Kim, Seong-Hyeon Hong. Improved moisture resistance of SrS:Eu²⁺ phosphors with nanoscale SiO₂ coating, *Journal of Luminescence*, 130(2010), 1400–1403.

64. R. Balakrishnaiah. Fluorescence properties of Er^{3+} -doped YPO_4 phosphors, ECS. 1(2009), 860.
65. Y. Lin. Surface characteristics of hydrous silica-coated TiO_2 particles, Journal of Powder Technology. 123(2002), 194–198.
66. M.L. Pang, J. Lin, M. Yu. Fabrication and luminescent properties of rare earths-doped $\text{Gd}_2(\text{WO}_4)_3$ thin film phosphors by Pechini sol–gel process, J. Solid State Chem. 177(2004), 2237–2241.
67. M. Yu. Silica Spheres Coated with $\text{YVO}_4:\text{Eu}^{3+}$ Layers via Sol–Gel Process: A Simple Method To Obtain Spherical Core–Shell Phosphors, Chem. Mater. 17(2005), 1783–1791.
68. A. Kioul, S. Mascia. Compatibility of polyimide-silicate ceramers induced by alkoxysilane silane coupling agents, J. Non-Cryst. Solids. 175 (1994), 169–186.
69. H. Sertchook and D. Avnir. Submicron Silica/Polystyrene Composite Particles Prepared by a One-Step Sol–Gel Process, Chem. Mater. 15 (2003), 1690–1694.
70. G. Blasse. Luminescent Materials, Springer verlag, Heiderlberg, 1994.
71. A.K. Levine, F.C. Palilla, A new highly efficient red emitting cathodoluminescent phosphor ($\text{YVO}_4:\text{Eu}$) for color television, Appl. Phys. Lett. 5(1964), 118–123.
72. F.C. Palilla and A.K. Levine. $\text{YVO}_4:\text{Eu}$: a Highly Efficient, Red-Emitting Phosphor for High Pressure Mercury Lamps, Applied Optics. 5(1966), 1467–1468.
73. K. Riwotzki, M. Haase. Colloidal $\text{YVO}_4:\text{Eu}$ and $\text{YP}_{0.95}\text{V}_{0.05}\text{O}_4:\text{Eu}$ Nanoparticles: Luminescence and Energy Transfer Processes, J. Phys. Chem. 105B (2001), 12709.

74. W.Y. Kang, J.S. Park, D.K. Kim, K.S. Suh. Pulsed-laser deposition of $\text{YVO}_4\text{:Eu}$ phosphor thin-films for low temperature fabrication Bull. Korean Chem.Soc. 22(2001), 921-924.
75. D. Wang, C. Huang, Y. Wu and T. Chen. $\text{BaZrSi}_3\text{O}_9\text{:Eu}^{2+}$: a cyan-emitting phosphor with high quantum efficiency for white light-emitting diodes, J. Mater. Chem. 21(2011), 10818–10822.
76. D. Cervantes-Vásquez, O.E. Contreras, G.A. Hirata, Quantum efficiency of silica-coated rare-earth doped yttrium silicate, J. Luminescence. 143 (2013), 226–232.
77. Y. Osawa, M. Haruta and K. Ohkubo. A study of quantum efficiency measurement for phosphor solutions, J. Ceram. Proc. Res. 14 (2013), 39-43.
78. C. Feldmann, T. Ju`stel, C.R. Ronda, D.U. Wiechert. Quantum efficiency of down-conversion phosphor $\text{LiGdF}_4\text{:Eu}$, J. Lumin. 92(2001), 245–254.
79. C. Zhang, et al. Effect of SiO_2 Coating on Photoluminescent Properties of Ca-alpha-SiAlON: Eu^{2+} Deposit Fabricated by Electrophoretic Deposition Process, ECS Solid State Letters. 2(2013), 23-26.
80. H.o Cui. Coating of $\text{Y}_2\text{O}_3\text{:Eu}^{3+}$ Particles with Alumina by a Humid Solid State Reaction at Room Temperature, J. Colloid and Int. Sci. 252 (2002), 184–187.
81. A. Bao, R. Haase. Luminescent properties of $\text{YVO}_4\text{:Eu/SiO}_2$ core–shell composite particles, J Nanopart Res. 12 (2010), 635–643.
82. R. Balakrishnaiah. Fluorescence properties of Er^{3+} -doped YPO_4 phosphors, ECS. 1(2009), 860.
83. D. Xing. A bluish green barium aluminate phosphor for PDP

- application, *Materials Letters*. 60(2006), 3217–3220.
84. S. Kim. Efficient Red Emission of Blue-Light Excitable New Structure Type $\text{NaMgPO}_4\text{:Eu}^{2+}$ Phosphor, *ECS Solid State Letters*. 12(2013), 49-51.
 85. L. Chen. Combinatorial chemistry approach to searching phosphors for white light-emitting diodes in (Gd-Y-Bi-Eu) VO_4 quaternary system, *J. Mater. Chem.* 21(2011), 3677-3685.
 86. Y. Fang. Energy Transfer and Thermal Quenching Behaviors of $\text{CaLa}_2(\text{MoO}_4)_4\text{:Sm}^{3+}, \text{Eu}^{3+}$ Red Phosphors, *Journal of the Electrochemical Society*. 158(2011), 1-5.
 87. W. Liu, Y. Chiu, Y. Yeh, S. Jang and T. Chen. Luminescence and Energy Transfer Mechanism in $\text{Ca}_{10}\text{K}(\text{PO}_4)_7\text{:Eu}^{2+}, \text{Mn}^{2+}$ Phosphor, *Journal of The Electrochemical Society*. 156(2009), 165-169.
 88. V. Bachmann, A. Meijerink, C. Ronda. Luminescence properties of $\text{SrSi}_2\text{AlO}_2\text{N}_3$ doped with divalent rare-earth ions, *Journal of Luminescence*. 129(2009), 1341–1346.
 89. C.T. Au, W.D. Zhang. Oxidative dehydrogenation of propane over rare-earth orthovanadates. *J. Chem. Soc., Faraday Transactions*. 93(1997), 1195-1204.
 90. M. Kruczek, E. Talik, H. Sakowska, W. Szyrski, Z. Ujma, D. Skrzypek. XPS investigations of $\text{YVO}_4\text{:Tm, Yb}$ single crystal. *J Cryst Growth*. 275(2005), 1715–1720.
 91. Y. Lu, Y. Yin, Z. Li and Y. Xia. Synthesis and Self-Assembly of Au@SiO_2 Core–Shell Colloids, *Nano Letters*. 7(2002), 785–788.
 92. V. Suryanarayanan, A. Sreekumaran Nair, Renjis T. Tom and T. Pradeep, Porosity of core–shell nanoparticles, *J. Mater. Chem.* 14(2004), 2661-2666.

93. F. Caruso. Nano-engineering of Particle Surfaces, *Advanced Materials*. 13(2001), 11–22.
94. W. Schärtl. Crosslinked Spherical Nanoparticles with Core–Shell Topology, *12(2000)*, 1899–1908.
95. A. E. Neeves and M. H. Birnboim. Composite structures for the enhancement of nonlinear-optical susceptibility, *JOSA B* 6(1989), 787–796.
96. G. Wakefield, E. Holland, P. J. Dobson and J. L. Hutchison. Luminescence Properties of Nanocrystalline $\text{Y}_2\text{O}_3\text{:Eu}$, *Advanced Materials*. 13(2001), 1557–1560.
97. S. H. Cho et.al. Cathodoluminescent characteristics of a Spherical $\text{Y}_2\text{O}_3\text{:Eu}$ Phosphor Screen for Field Emission Display Application, *J. Electrochem. Soc.* 147(2000), 3143–3147.
98. X. Jing. Control of $\text{Y}_2\text{O}_3\text{:Eu}$ Spherical Particle Phosphor Size, Assembly Properties, and Performance for FED and HDTV, *J. Electrochem. Soc.* 146(1999), 4654–4658.
99. H. Wang, M. Yu. Core–shell structured $\text{SiO}_2\text{:YVO}_4\text{:Dy}^{+3}\text{Sm}^{+3}$ phosphor particles: Sol–gel preparation and characterization, *Journal of Colloid and Interface Science*. 300(2006), 176–182.
100. C. Lin, D. Kong, X. Liu, H. Wang, M. Yu and J. Lin. Monodisperse and Core–Shell-Structured $\text{SiO}_2\text{:YBO}_3\text{:Eu}^{3+}$ Spherical Particles: Synthesis and Characterization, *Inorg. Chem.* 46(2007), 2674–2681.
101. H. Wang, M. Yu, C.K. Lin, J. Lin. Core–shell structured $\text{SiO}_2\text{:YVO}_4\text{:Dy}^{3+}\text{Sm}^{3+}$ phosphor particles: Sol–gel preparation and characterization, *J of Colloid. Inter. Sci.* 300(2006), 176–182.
102. M.L Pang, J. Lin. Fabrication and luminescent properties of rare earths-doped $\text{Gd}_2(\text{WO}_4)_3$ thin film phosphors by Pechini sol–gel process, *Journal of Solid State Chemistry*. 177(2004), 2237–2241.

